University of Groningen
Faculty of Mathematics and Natural Sciences
Zernike Institute for Advanced Materials

Photophysical Properties of Solution Processable Hybrid Semiconductors

Mustapha Tisan Abdu-Aguye

August 2014

Supervisor:

Prof. dr. M.A. Loi

A thesis submitted in fulfilment of the requirements for the degree of M.Sc. Nanoscience

Photophysics and Optoelectronics
Zernike Institute for Advanced Materials
University of Groningen

Abstract

Recently, several new hybrid materials have been explored for photovoltaic applications because they exhibit favourable qualities typical of inorganics (high stability, good carrier mobilities) as well as organics (solution processability & low cost). One of such materials, namely, ternary **$CuInS_2$ (CIS) nanocrystals and CIS/ZnS core-shell nanocrystals** are promising alternatives to the non-environmentally friendly Lead and Cadmium based nanocrystals predominantly used in colloidal solar cells. Bulk CIS is a direct band gap semiconductor with good absorption and emission properties, as well as high photoconductivity. We show that for CIS and CIS/ZnS nanocrystals increasing the stoichiometric amount of Indium leads to an increase in band-gap and consequently a blue-shift in absorption & photoluminescence for both core-only and core-shell particles, with an increase in the magnitude of the blue shift for the core shell samples. We also observe large FWHM in their emission, and tentatively ascribe it to radiative recombination arising from intrinsic Cu-vacancy sites via a donor-acceptor pair transition. Furthermore, time-resolved photoluminescence measurements reveal fluorescence lifetimes of around 200 - 300 ns, one order of magnitude shorter than other colloidal nanocrystals such as PbS/OA in solution; we interpret this as an indication that material quality is still sub-optimal; thus, further refinement of synthetic techniques are still required

Another interesting family of materials in this class are hybrid perovskites of which $(CH_3NH_3)PbI_3$ ($MAPbI_3$) is a typical member and has recently been shown to exhibit exceptional power conversion efficiencies in solar cells as high as 17.9% (NREL). We report the facile and successful synthesis of **single crystals of $MAPbI_3$** from MAI and PbI_2; confirmed by powder XRD, and show the signature of a tetragonal-orthorhombic phase transition in both variable temperature single crystal XRD and Steady State Photoluminescence Spectroscopy; which initially shows a temperature dependence of the band gap. We observe unusual changes in steady state photoluminescence spectra between 150K and 30K which we further investigate by power dependent measurements. Furthermore, Photoluminescence lifetime shows an almost 60-fold increase between room temperature and 5K indicating a high photoexcitation efficiency.

Finally, we conclude by relating these observations to recent theoretical results by Even et al by proposing tentative explanations to these phenomena in terms of a multi bandgap electronic structure.

Contents

List of Tables and Figures

Part I

The Effects of Cu-deficiency and a ZnS shell on the Photophysical Properties of Ternary $CuInS_2$ (CIS) Nanocrystals

Chapter 1

Introduction

This chapter contains a basic introduction to semiconductor Nanocrystals or "Quantum Dots" as they are more commonly known; outlines why ternary $CuInS_2$ Nanocrystals are desirable over the mainly studied II-IV family (of which PbS and CdSe are typical examples), gives some of their properties that make them interesting for applications and finally gives the motivation for this part of my thesis.

1.1 Basics of Colloidal Nanocrystals

Inorganic semiconductor nanocrystals (NCs) are crystalline aggregates (hundreds to a few thousand) of atoms, considering the Å-size of each atom; each NC is sized between 1-10 nm. The exciting properties of NCs that have made them the object of much research in the past decade are centred on their excellent optical and electronic properties and size-tunable band gap. In addition, their colloidal synthesis makes it possible to conceive of using them for cheap, large-scale applications as varied as photodetectors, light-emitting devices, solar-cells and even in biological systems as drug-delivery agents and fluorescent labels.

From a physical point of view NCs have dimensions which are generally smaller than the distance of an electron-hole pair - the so-called *exciton*-Bohr radius. This is the reason why their electronic properties become strongly-size dependent, with the band gap becoming progressively larger as their size decreases. This effect is commonly referred to as the *Quantum Confinement effect*. Therefore, NCs show properties intermediate between single molecules and bulk solid, with excitons confined in all three spatial dimensions and a delta-function peaked *density of states*. For this reason, NCs are sometimes called "Quantum Dots"

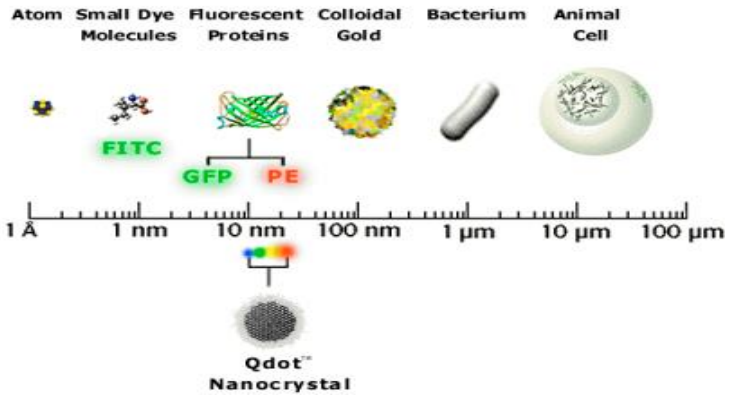

Figure 1.1(a): Nanocrystal sizes in comparison to other microscopic structures (Credit: www.nanotech-now.com)

1.2 Effects of Quantum Confinement

As mentioned earlier, nanoscale semiconducting materials such as NCs fall into the "Quantum confinement" regime where excitons are confined in all three dimensions; this results in a size-controlled discretization of the energy levels as compared to the continuous valence and conduction band of bulk materials.

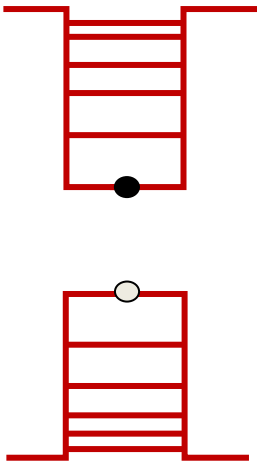

Figure 1.2(a): Quantum Confinement results in a discretization of energy levels and increases the band gap from the bulk value

The relationship between the Bandgap of a NC and the bulk material, was derived by L. Brus [7]; is given by the analytical expression:

$$E_g^{NC} = E_g + \frac{\hbar^2\pi^2}{2R^2}\left(\frac{1}{m_e} + \frac{1}{m_H}\right) - \frac{1.8e^2}{\varepsilon_0 \varepsilon R} \qquad (1.2.1)$$

Where E_g^{NC} and E_g represent the energy band gaps of the NC and bulk semiconductor respectively; R, ε, m_e and m_H represent the radius, relative permittivity and effective masses of electrons (e) and holes (h); and $\varepsilon_0, \hbar$ and e are as usual, the vacuum permittivity, reduced Planck constant and elementary electronic charge. Equation $(1.2.1)$ shows the effect of reducing the NC size on the quantum confinement energy (second term) and associated Coulomb attraction of the electron-hole pair (third term); when R becomes sufficiently small, the second term outweighs the third which

results in an increase of E_g^{NC}; and a hypsochromic (high energy) shift in absorption and emission from the NC compared to the bulk.

Thus, using simple synthetic strategies, it is possible to tailor the absorption and emission properties of NCs over a wide range from the infrared (IR) to ultraviolet (UV), thus they are highly desirable for applications such as solar cells, photodetectors and biological labels.

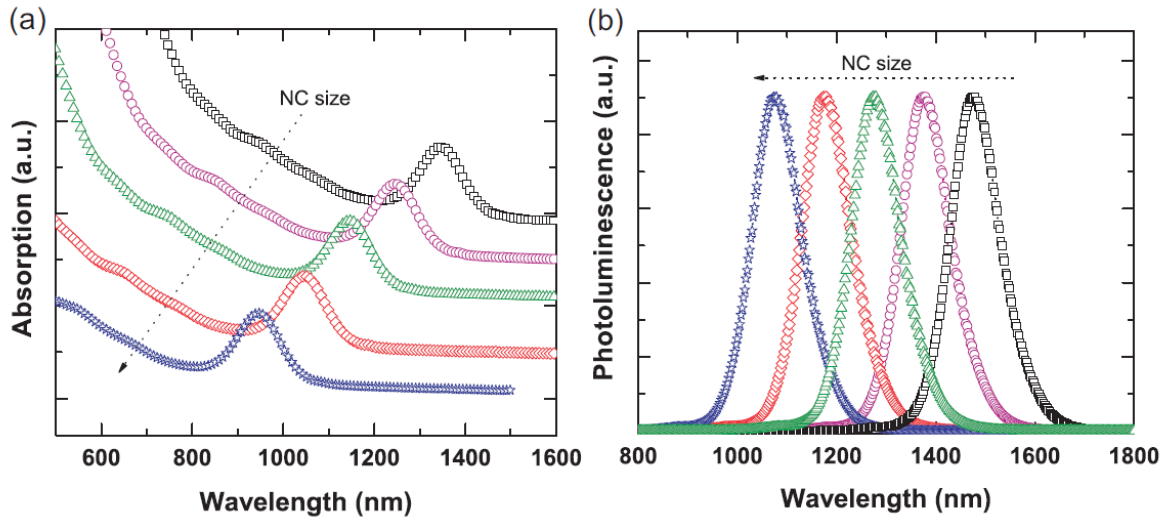

Fig 1.2(b): size dependence of absorption (a) and emission (b) in PbS Nanocrystals from [6]. Suitable synthetic approaches can be used to tailor prooperties to the desired application

However, there are several challenges that have to be addressed before the use of NCs is actualised for highly efficient, commercializable, photovoltaic applications. One of which is that several of the more commonly studied nanoparticles, the Lead Chalcogenide based PbS, PbTe and their Cadmium-based analogues CdS, CdSe and CdTe; while having excellent physical properties, are toxic and not therefore environmentally friendly. As alternatives, III-V, I-III-VI NCs have been suggested by several research groups. Part of this thesis covers the optical properties of $Cu_xIn_{1-x}S_2$ (CIS) NCs – a representative member of the I-III-VI family obtained by varying the ratio of Cu precursor to In precursor during synthesis, and also the effect a Zinc Sulphide (ZnS) shell on the photoluminescence spectra and fluorescence lifetime.

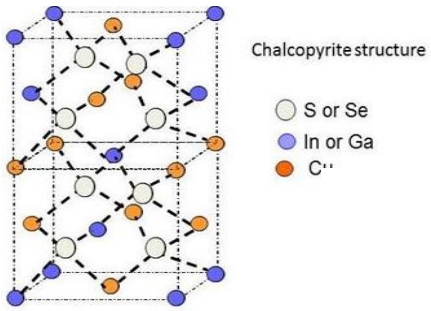

Fig 1.2(c): Chalcopyrite structure of $CuInS_2$

Another challenge is the removal of the long insulating ligands that are used to both stabilize & solubilize the NCs during synthesis because they hinder charge transport, as with the Pb and Cd-based NCs where several strategies have already been established. The CIS NCs used in this study were synthesized with the capping ligand Dodecanethiol (DDT).

1.3 Motivation and Goals

CIS NCs have been hitherto mostly unstudied compared to the non-environmentally friendly PbS and CdSe, with the few reported studies focusing on synthesis and structural characterization rather than device applications. Bulk CIS is an important material for photovoltaic applications because it has a high absorption coefficient and photoconductivity [8]. In addition, the presence of a ZnS shell and varying Cu:In ratios have only recently become interesting for studies, particularly for applications in (opto)electronics and photovoltaics.

Another motivation for this project is the lack of optimization of the synthetic procedure for the controllable synthesis of high quality, mono-disperse CIS and CIS/ZnS NCs; several studies in literature report a wide array of techniques including hot injection, thermal decomposition etc. with varying degrees of success and sometimes conflicting reports. Thus, with the optical measurements of the CIS synthesized by our collaborators at ETH Zurich by absorption, steady-state and time-resolved photoluminescence spectroscopy, we not only gain insights about the effects of non-stoichiometry and a ZnS shell on the photophysical properties; but also about material quality and the efficacy of the synthetic protocol. The final goal would then be to optimize the material quality, and thin film deposition techniques for making devices such as solar cells.

Chapter 2

Materials and Methods

This chapter gives an overview about the synthesis of the ternary CIS NCs used in this thesis. Furthermore, a brief explanation of the techniques used to study the optical properties is given.

2.1 Synthesis of NCs

The CIS NCs were prepared by a non-injection, thermal decomposition route following procedures reported in [5], [9] and [10]. Briefly, the method involves the decomposition of precursors: Copper(I) Iodide (CuI), Indium(III) Acetate ($In(oAC)_3$), Dodecanethiol (DDT), Octadecene (ODE), and Oleic acid (OA); followed by purification involving centrifugation in Ethanol (or Acetone) and then dispersion in Chloroform. For the Zinc Sulphide shell overcoating, a stock solution using Zinc Stearate (or Acetate), DDT and ODE (or Oleylamine) is added dropwise during the growth of the CIS core and left for 60-70 minutes before purification.

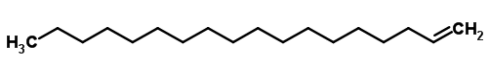

Octadecene

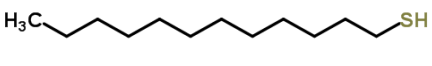

Dodecanethiol (DDT)

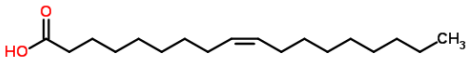

Oleic acid

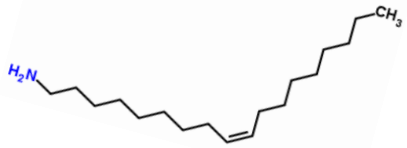

Oleylamine

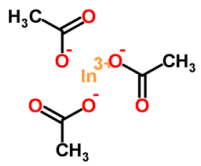

Indium(III) acetate

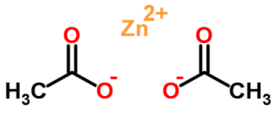

Zinc acetate

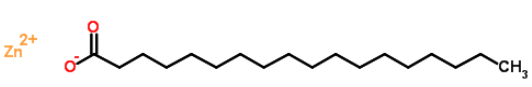

Zinc stearate

Fig 2.1(a): Molecular structures of Precursors used for synthesis

S/n	Sample	Cu:In feed ratio	Precursors
1	$CuInS_2$	1:1	Core: CuI, $In(OAc)_3$, DDT, ODE, OA Purification: Acetone/Chloroform
2	$CuInS_2$/ZnS	1:1	Core: CuI, $In(OAc)_3$, DDT Shell: Zn-stearate, DDT, ODE Purification: Ethanol/Chloroform
3	$CuInS_2$	1:2	Core: CuI, $In(OAc)_3$, DDT Purification: Ethanol/Chloroform
4	$CuInS_2$/ZnS	1:2	Core: CuI, $In(OAc)_3$, DDT Shell: Zn-stearate, DDT, ODE Purification: Ethanol/Chloroform
5	$CuInS_2$	1:4	Core: CuI, $In(OAc)_3$, DDT Purification: Ethanol/Chloroform

Table 2.1 (a): Summary of samples synthesized and precursors used

2.1.1 Solutions and handling

All solutions were prepared in a clean Nitrogen-filled glove box to avoid contamination by atmospheric oxygen and moisture. 400uL of solution at concentrations ranging from (2.37mg/ml to 9.5mg/ml) were put into 1cm quartz cuvettes and sealed before removal from the glove box. Measurements were carried out in ambient atmosphere.

2.2 Absorption Measurements

Absorption spectroscopy is a technique that gives information about transitions between electronic states of material with the specific energies where the transitions occur being dictated by the electronic structure of the particular material [6]. Following optical excitation, NCs are promoted from their electronic ground state (S_0) to an electronic excited state (S_n) which is usually the first singlet excited state (S_1). Immediately after, (ultra)fast processes i.e. both non-radiative (thermal relaxation), or radiative (recombination to S_0) on a picosecond (ps) time scale or slower may occur.

Every spectrophotometer generally consists of a light source, a monochromator and a detector. It should however, be noted that a spectrophotometer does not measure "absorption" directly but

rather transmitted light after excitation of the sample and its interaction with the excitation. Using the Beer-Lambert law (equation 2.2) below:

$$I = I_0 e^{-\alpha d} \qquad (2.2)$$

Where I is the transmitted light through the sample, I_0 is the incident radiation. α and d represent the attenuation coefficient and the distance the light travels through the material (often defined by the size of sample holder) respectively; the intensity of transmitted radiation (T) is then related to the Absorbance also loosely called "optical density" via:

$$A = -\log_{10}\left(\frac{I}{I_0}\right) = -\log_{10} T \qquad (2.3)$$

Our samples were measured with a Shimadzu-3600 UV/VIS/NIR spectrophotometer in the spectral range between 300 nm – 900 nm.

2.3 Steady State Photoluminescence (PL) Spectroscopy

PL measurements are an especially powerful tool to investigate the electronic excited states of molecules; they can give information about interaction between photogenerated excitons and capping ligands, as well as the local environment, for instance the presence of defects or trap states; provided the recombination from them is radiative.

For our measurements, we used the second harmonic of a 150fs mode-locked Ti:Sapphire laser at 795 nm with a repetition rate of ca. 76 MHz, pumped by a solid-state, diode-pump frequency doubled Nd:Vanadate (Nd:YVO_4) laser at 532 nm with an output power of 5 Watts. All spectra were collected by a Hamamatsu EM-CCD camera working in the visible range and corrected for the spectral response of the setup with a calibrated lamp

2.4 Time resolved Photoluminescence (TRPL) Spectroscopy

TRPL spectroscopy is one very powerful method to investigate the dynamics of processes after excitation; as implied by the name, it involves measuring the PL from a sample as a function of time

after excitation by a pulsed (monochromatic) source. Using this technique, valuable information about dynamic processes such as variation of excited populations due to energy loss, charge transfer or other interaction of the excitation with the surroundings can be obtained

For NCs in general, replacing the native insulating ligands by shorter, conductive ligands results in a significant reduction of the decay time from the order of several tens or hundreds of nanoseconds (ns) to picoseconds (ps), this is often ascribed to increased interaction through the electronic levels of the ligand molecules between nanoparticles, which enables charge transfer [6].

For our measurements the same laser system described above was used, and time resolved spectra were collected with a Hamamatsu streak camera with a photocathode sensitive in the visible range, working in single sweep mode, together with an optical pulse selector with a division ratio set to 1:100.

Chapter 3

Results and Discussion

3.1 CIS Core-Only NCs

3.1.1 Absorption Measurements

The figure 3.1.1 below shows the absorption of CIS core-only NCs in the spectral range between 300-900nm for NCs with different Cu:In composition ratios. From the spectra, it is evident that the absorption is blue-shifted (towards visible wavelengths) as the stoichiometric ratio of Indium (In) increases. Similar behaviour has been reported by Song et al [10], which they explained in terms of lowering of the valence band due to decreased repulsion between Cu d-orbitals and S p-orbitals; based on calculations performed for Cu-deficiency in $CuInSe_2$; resulting in a bandgap widening [12]. Visually the colors of the solutions can be observed changing from (deep) red for Cu:In of 1:1 ratio to orange (fig 2) for the 1:4 ratio.

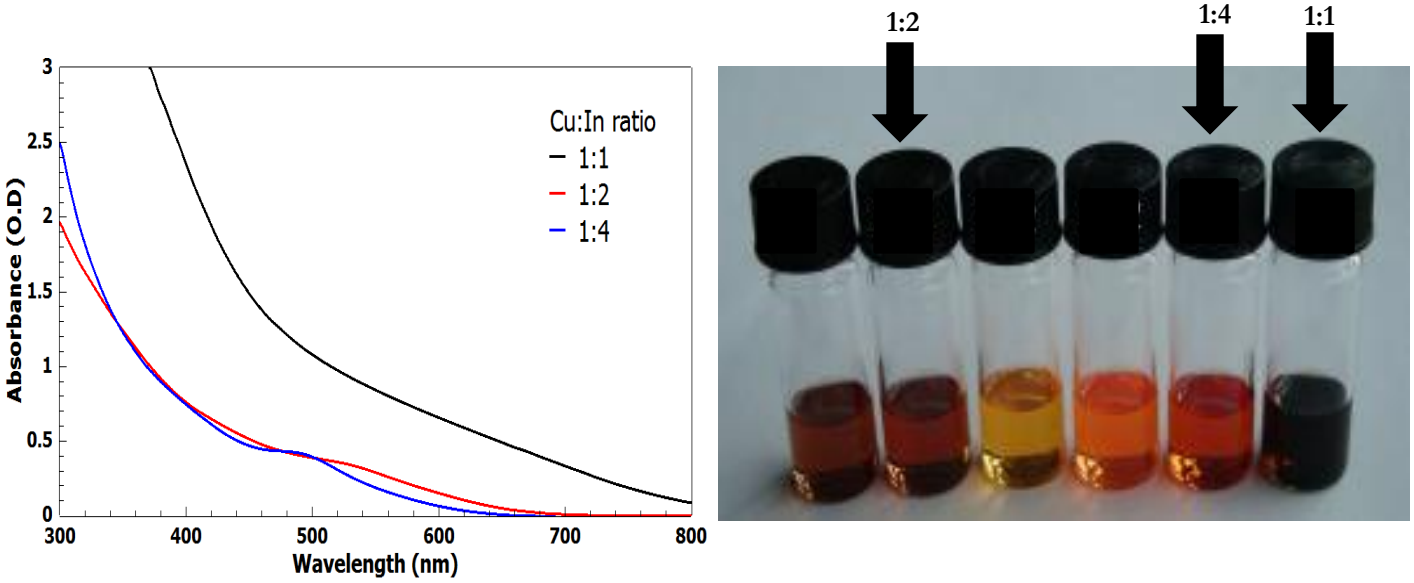

Figure 3.1.1(a): Absorption spectra for CIS core-only NCs with different Cu:In ratios; (b) Picture of synthesized samples, arrows indicate core-only samples

Also, the 1:1 ratio (black line) does not show a clear excitonic peak but rather a "shoulder"; this might be an intrinsic property of CIS, or due to inhomogeneities in the size, shape and composition of our sample [16].

3.1.2 Steady state Photoluminescence Measurements

Figure 3 below shows the spectra for the CIS core only NCs with different Cu:In ratios, the same trend observed in the absorption measurements is observed here, with the emission progressively blue shifted as the stoichiometric amount of In increases consistent with a wider band gap for increasing amounts of Cu deficiency in our samples. Our results and several studies [5,8,10,16] report a large emission bandwidths which most likely stem from Cu-deficiencies, S-vacancies and Cu-In substitution (defect sites) which serve as intra-gap states; implying a donor-acceptor pair (DAP) recombination as a possible mechanism for this occurrence rather than an excitonic emission; where In substituted at the Cu site and/or an S vacancy likely act as donor states and a Cu vacancy as an acceptor state [10]; another possibility proposed by Nose et al [13] is recombination between the conduction band minimum (CBM) and an acceptor (defect) level as observed in $CuInSe_2$ NCs.

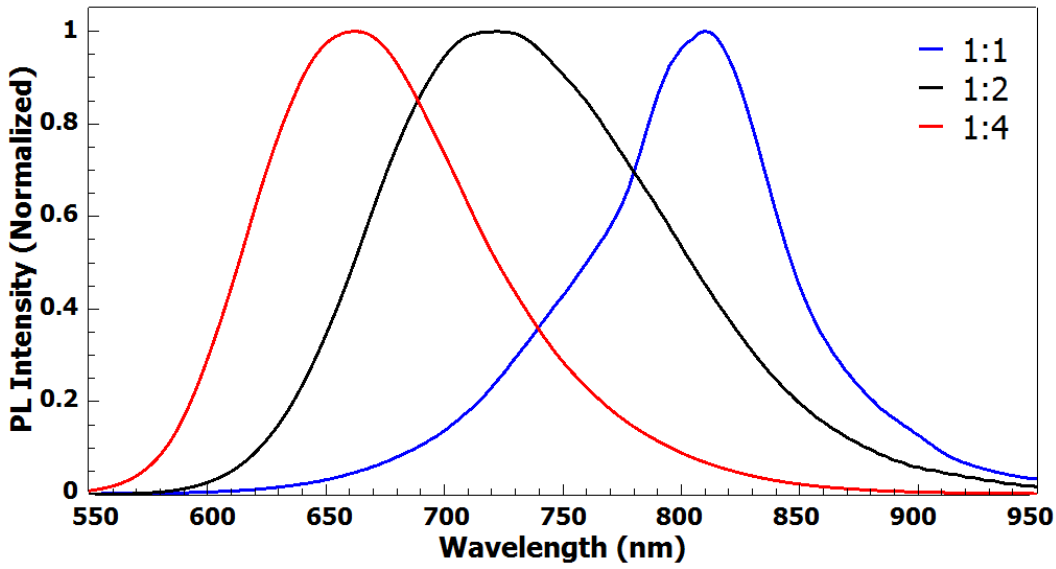

Figure 3.1.2(a): Normalized PL Spectrum for CIS core-only NCs with different Cu:In ratios, to illustrate the blue shift in emission with increasing Cu defiency, Excitation intensity is ca. 40uW

Further evidence for the defect-related radiative recombinations are the somewhat large stokes shifts, though we note also that our samples contain pyramidal NCs of poly disperse size; thus we expect both phenomena play a role in the large emission bandwidths

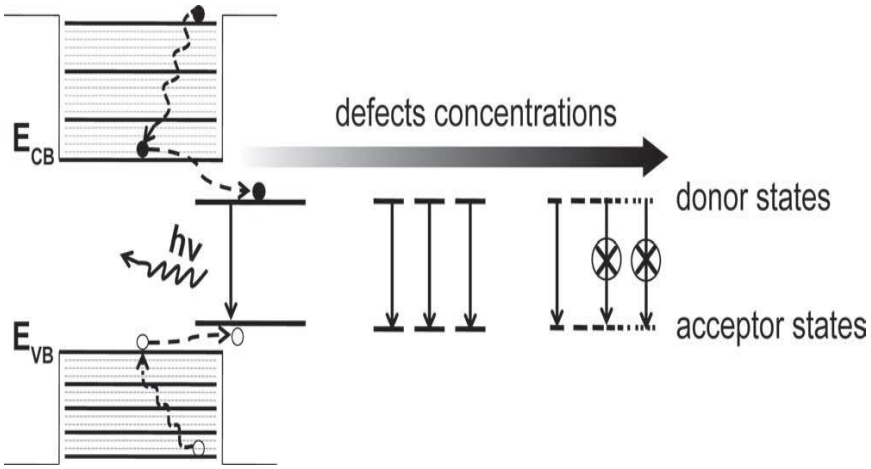

Figure 3.1.2(b): Schematic diagram explaining the DAP recombination mechanism mentioned above, interestingly it predicts that PL quenching can occur when the concentrationof D and A states becomes so large that interactions begin to occur between them. Figure adpated from [40]

3.1.3 Time-Resolved Photoluminescence Measurements

The decay times for the PL from our samples were also measured to ascertain if there were any significant differences in the fluorescence lifetimes as a function of Cu:In ratio, our results indicate that the lifetimes display an increasing trend with increasing Cu:In ratios with the intensity exhibiting multi-exponential decay behaviour well fitted by the equation

$$I(t) = \sum_{i=1}^{n} a_n \, exp^{\frac{-t}{\tau_n}}$$

Table (3.1.3) shows a summary of the extracted lifetimes and Figures (a)-(c) below show the spectra and (multi) exponential fits

S/N	Sample	Cu:In Ratio	n	Extracted Lifetimes
1	$CuInS_2$	1:1	2	$\tau_1 = 44ns$ $\tau_2 = 242ns$
2	$CuInS_2$	1:2	2	$\tau_1 = 33ns$ $\tau_2 = 253ns$
3	$CuInS_2$	1:4	1	$\tau = 210ns$

Table 3.1.3(a): PL decay lifetimes for CIS core-only NCs

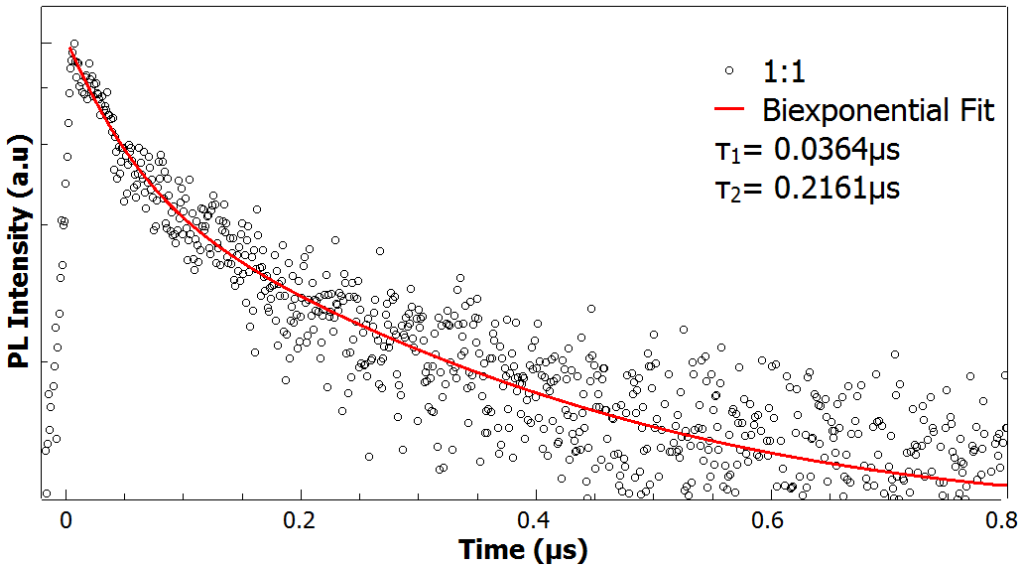

Figure 3.1.3(a): PL decay for CIS core-only NC with Cu:In ratio 1:1, hollow circles are experimental data and the red line is a Biexponential fit of the data. Excitation intensity is ca. 80uW

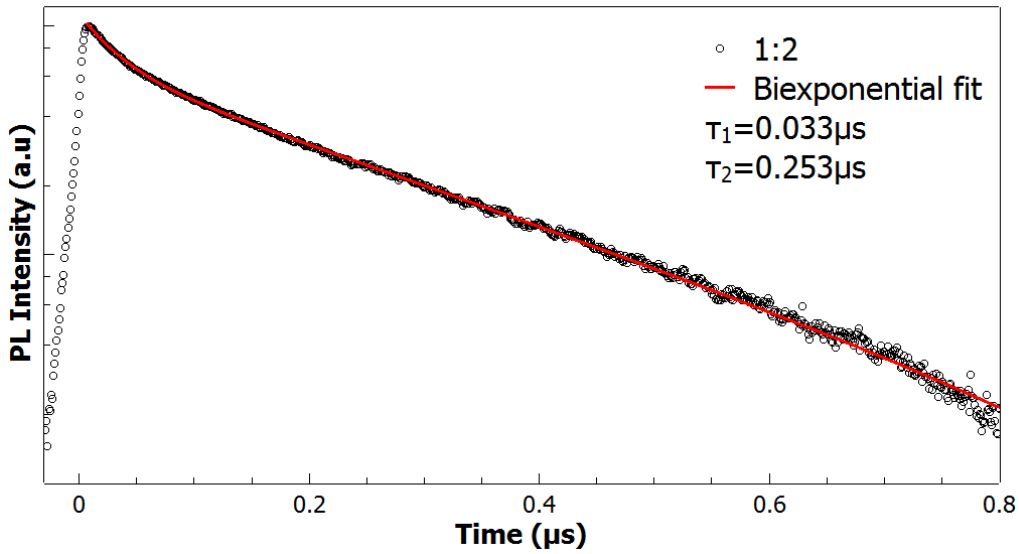

Figure 3.1.3(b): PL decay for CIS core-only NC with Cu:In ratio 1:2, hollow circles are experimental data and the red line is a Biexponential fit of the data. Excitation intensity is ca. 80uW

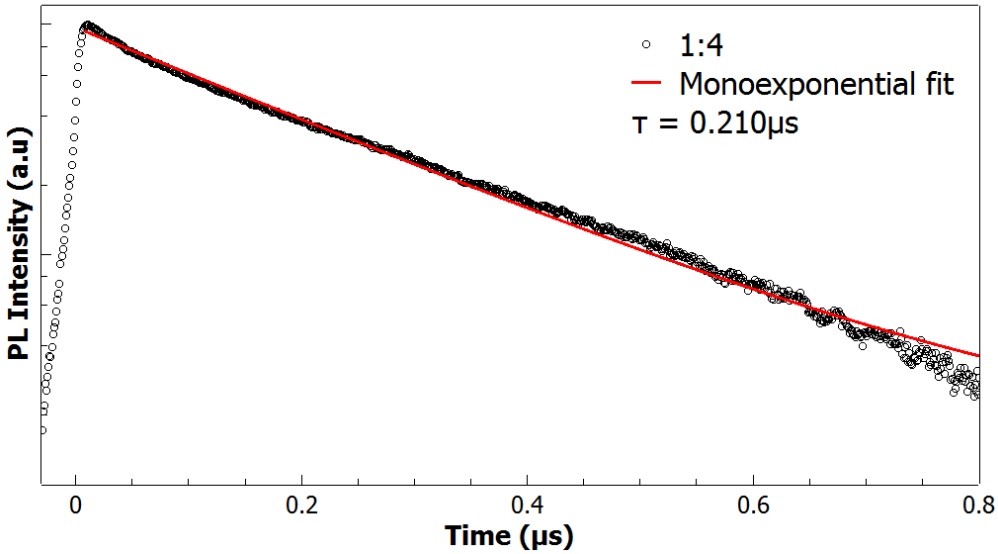

Figure 3.1.3(c): PL decay for CIS core-only NC with Cu:In ratio 1:4, hollow circles are experimental data and the red line is a Biexponential fit of the data. Excitation intensity is ca. 80uW

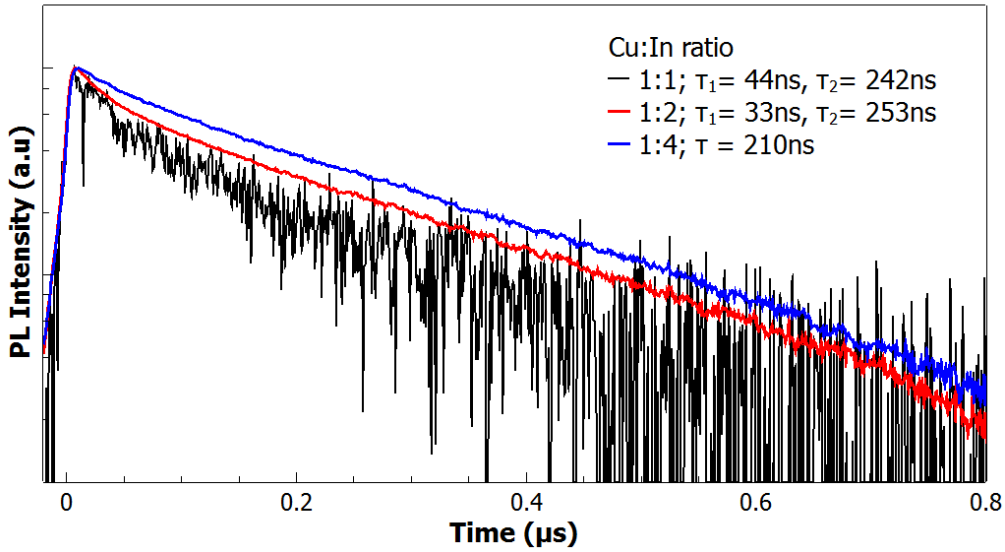

Figure 3.1.3(d): Lifetime comparison for different Cu:In ratios, lifetime increases with increasing amounts of In

3.2 CIS/ZnS Core-Shell NCs

The growth of an overlayer of a higher bandgap material around NCs has been proven to result not only in better surface passivation but also in superior optical properties such as higher PL quantum yield, and improved stability [4]. ZnS is an ideal material for use as a shell for CIS, owing to its large

band gap relative to CIS ($3.6eV$ relative to ~$1.5eV$) resulting in type-I band alignment, similarity of crystal structure and low lattice mismatch (ca. 3%); its chemical stability and non-toxic character [5].

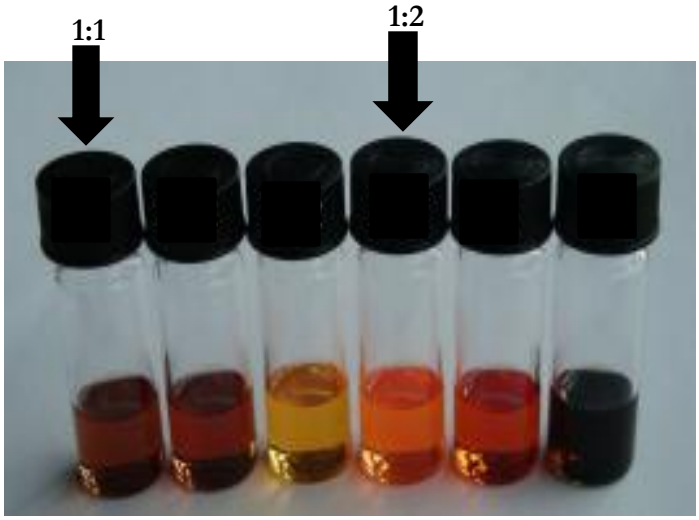

Figure 3.2(a): As synthesized core-shell Nanocrystals, arrows indicate Cu:In ratios

3.2.1 Absorption Measurements

The figure below shows the absorption spectra for the CIS/ZnS core-shell NCs for cores with different Cu:In ratios; the presence of the shell does not seem to significantly alter the absorption spectra. We observe the same general trend with the core-only NCs: no clear excitonic peak for the 1:1 ratio and a blue shifted absorption for the higher Cu deficient sample.

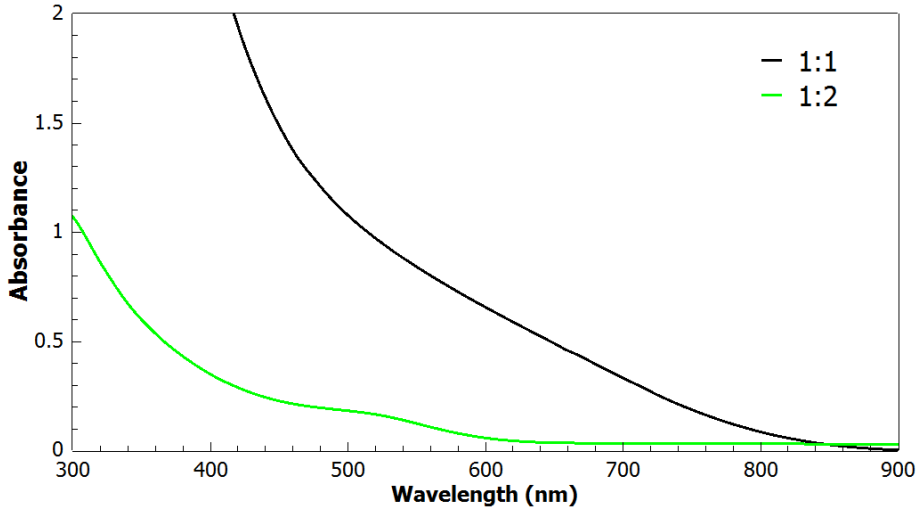

Figure 3.2.1(a): Absorption Spectra for CIS/ZnS core-shell NCs with different Cu:In ratios

3.2.2 Steady State Photoluminescence Measurements

We observe a further blue shift in PL emission from the core-shell samples, with a magnitude larger than that for the core only particles, suggesting that the band-gap is widened by the growth of the ZnS shell.

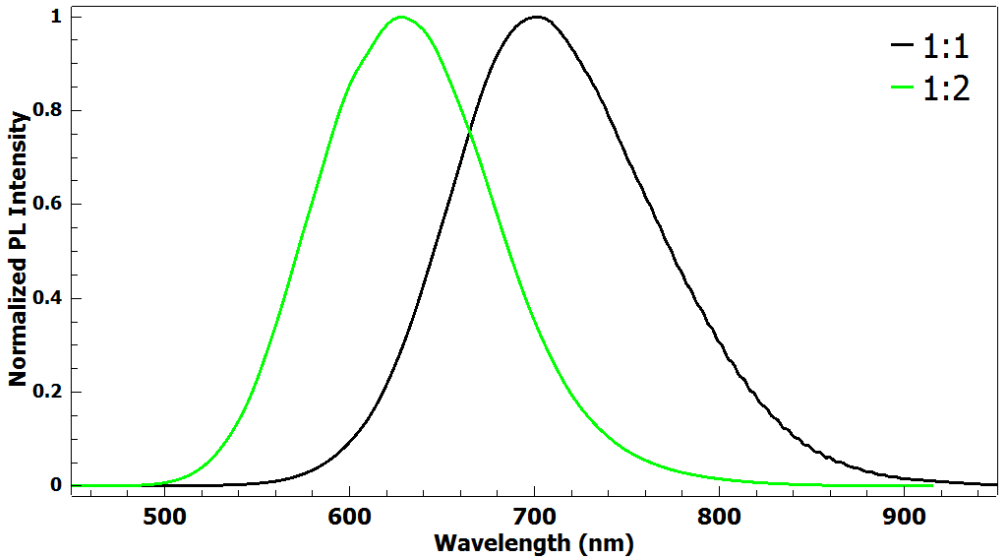

Fig 3.2.2(a): Normalized PL spectra for CIS/ZnS core-shell NCs with different Cu:In ratios illustrating the blue shift with increasing In compositon, excitation intensity is ca. 40uW

In addition, the emission features a broad bandwidth broader than the typical few kT bandwidth typical of band edge photoluminescence, suggestive of size poly dispersity and the presence of PL from defect states. Studies in literature have explained this blue shift by various arguments such as surface reconstruction [17], interdiffusion of Zn atoms to form a CIS-ZnS alloy around the surface [18], bandgap widening via compressive strain resulting from a lattice mismatch between CIS and ZnS; and even etching of the CIS core under growth conditions; However, subsequent experiments by Park and Kim [4] assert that that cation exchange is the main mechanism through which the growth of the ZnS overcoating occurs, which seems to be the most convincing explanation since this effectively reduces the core size and consequently explains the blue shifted PL.

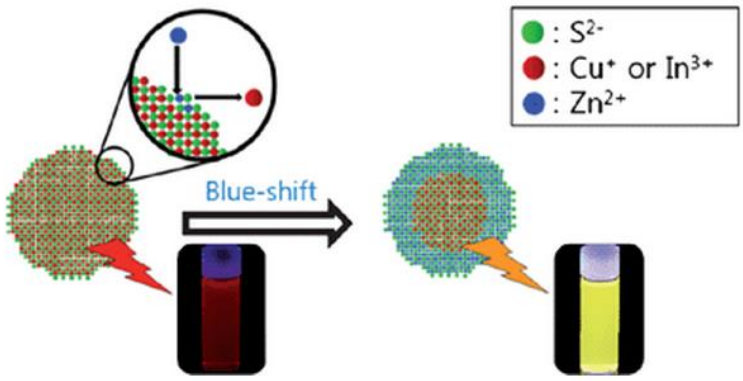

Fig 3.2.2(b): Shell growth mechanism involving replacement of Cu^{2+} and In^{3+} ions with Zn^{2+} ions, effectively reducing the core size and increasing the bandgap. Figure adapted from [4]

3.2.3 Time-Resolved Photoluminescence Measurements

In order to investigate the effect of the ZnS shell on the PL of the core-shell NCs the PL decay lifetime was measured. We observed a general multi-exponential behaviour similar to the core-only NCs; however, there was a slight increase in the PL lifetime, consistent with better surface passivation provided by the ZnS shell. Below are the extracted lifetimes for the samples.

S/N	Sample	Cu:In Ratio	n	Extracted Lifetimes
1	$CuInS_2/ZnS$	1:1	1	$\tau = 300ns$
2	$CuInS_2/ZnS$	1:2	2	$\tau_1 = 30ns$ $\tau_2 = 274ns$

Table 3.2.3(a): PL decay lifetimes for the CIS/ZnS core-shell samples

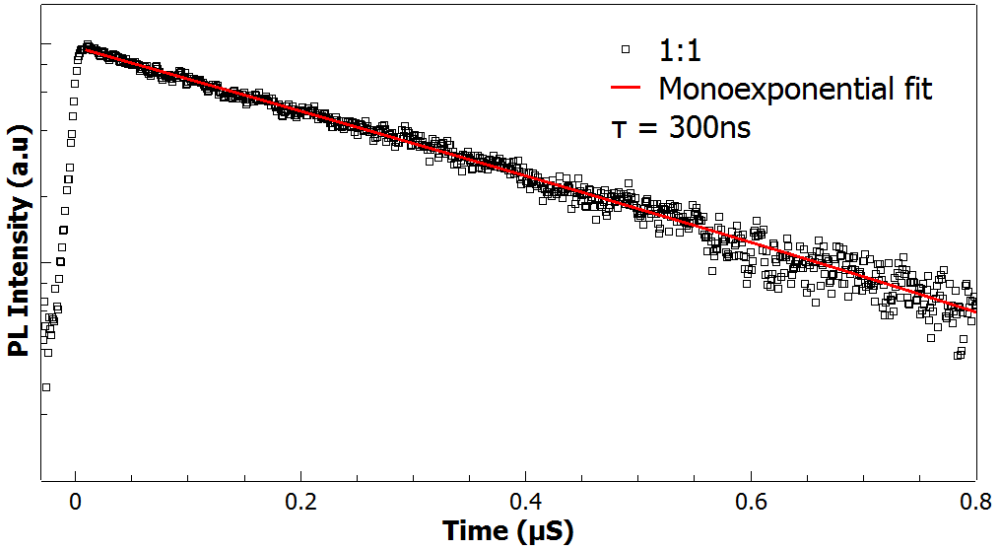

Figure 3.2.3(a): PL decay for CIS/ZnS core-shell NC with Cu:In ratio 1:1, hollow squares are experimental data and the red line is a monoexponential fit of the data. Excitation intensity is ca. 7.5uW

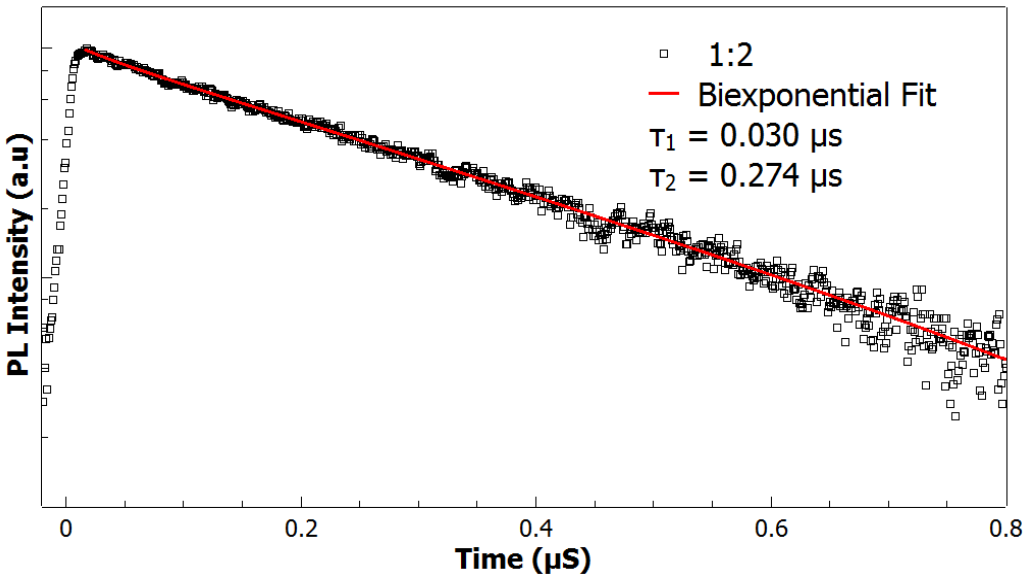

Figure 3.2.3(b): PL decay for CIS/ZnS core-shell NC with Cu:In ratio 1:2, hollow squares are experimental data and the red line is a biexponential fit of the data. Excitation intensity is ca. 7.5uW

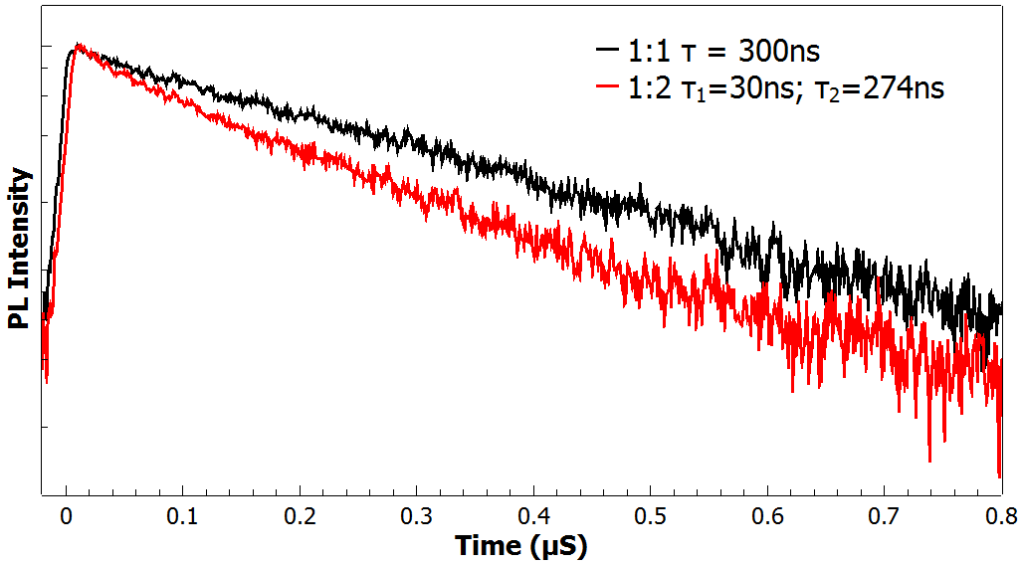

Figure 3.2.3(c): Lifetime comparison for CIS/ZnS core-shell samples with different Cu:In ratios, lifetime increases compared to core-only samples

Chapter 4

Conclusion and Outlook

Cadmium and Lead Free Ternary CIS NCs with high quality and promising optical properties were synthesized. We studied the effects of varying stoichiometric ratios of Cu:In and can conclude that the absorption and emission properties are strongly blue shifted by increasing the amount of In, relative to Cu. This further gives yet another method to engineer the properties of CIS (or more generally, ternary) NCs for different applications. We also observed broad emission bandwidths and long PL decay lifetimes from our samples indicative of size poly dispersity, and delayed emission from intrinsic defects in the CIS system

Furthermore, we studied the effect of growing a ZnS shell on the CIS NCs, our results show that the PL intensity is greatly improved by the presence of the ZnS shell, likely arising from the type I band alignment between the energy levels of CIS and ZnS and better surface passivation; which also resulted in a slightly longer PL lifetime. The blue-shifted emission for these samples is explained as a bandgap widening resulting from cation exchange during the shell growth process.

From an application viewpoint, the broad bandwidth of emission implies that CIS NCs would not be useful for display applications, where an extremely narrow emission linewidth is a requirement, but the tunable, high absorption and emission in the visible range makes them promising candidates for use in white LEDs as fluorescence down-converters in combination with a blue LED-chip [10]. Another possible niche for CIS NCs is as an absorber in tandem solar cells, where up till now, organics are still the mainstay for sub cells absorbing in the visible region. However, material quality is still sub-optimal and requires great improvement.

Our future efforts will be geared towards the optimization of material quality to obtain high quality, stable and mono-disperse NC populations, thin film deposition techniques, ligand exchange and the fabrication of transistors and solar cells to test the efficiency of the CIS NCs in devices.

Part II

Low Temperature Photophysical Properties of Single Crystals of the Hybrid Perovskite (CH_3NH_3)PbI_3 ($MAPbI_3$)

Chapter 5

Introduction

5.1 Motivation

Lead chalcogenide based hybrid Perovskites have recently taken the photovoltaic research community by storm starting by the report by Miyasaka and co-workers showing a 3.8% efficiency of solar cells made from $MAPbI_3$ [23] in a dye-sensitized geometry, between then and now – several advances in film processing, device architectures and suitable charge extraction strategies have seen efficiencies of Perovskites based solar cells rise to an impressive 19% so far, with the likelihood of even higher figures in the future [20, 34].

Interestingly, though hybrid Perovskite-based photovoltaic research is still in its infancy and as serious contenders for possible commercialization, already in competition with leading second generation solar cells, there is a marked lack of understanding of the basic physical properties that are responsible for such stellar device performance, the "gold-rush" for high efficiencies has unfortunately pushed such investigations to the back seat and as such; literature about the physical and (opto)electronic properties are lacking vis-à-vis understanding the origin of device operation and performance.

Reports in literature [27,34] and experience in our group indicate that organic-inorganic hybrid Perovskites are difficult materials to process into thin films for device applications; and being hybrid materials (consisting of a lead chalcogenide and organic ligand), simply applying known techniques for well-studied organic polymers is not sufficient for making good films into working devices. Our concern however, lies in the characterization of the physical and (opto) electronic properties of Perovskite **single crystals** via photoluminescence spectroscopy at low temperatures to gain some insight about elementary photo-excitations and how they translate into device operation. In addition, we have focused all our studies on methyl-ammonium lead iodide $(CH_3NH_3)PbI_3$ (=$MAPbI_3$)

5.2 Physical Properties and Structure

Perovskites are a class of materials that adopt the same structure as Calcium Titanate ($CaTiO_3$) with a general formula ABX_3, A and B represent cations which may be of different valence or ionic radius and X is often oxygen or a halogen. Replacement of the A cation by a suitable organic moiety such

as methyl ammonium (MA) or butyl ammonium (BA) leads to a sub-class of organic-inorganic hybrid Perovskites [19].

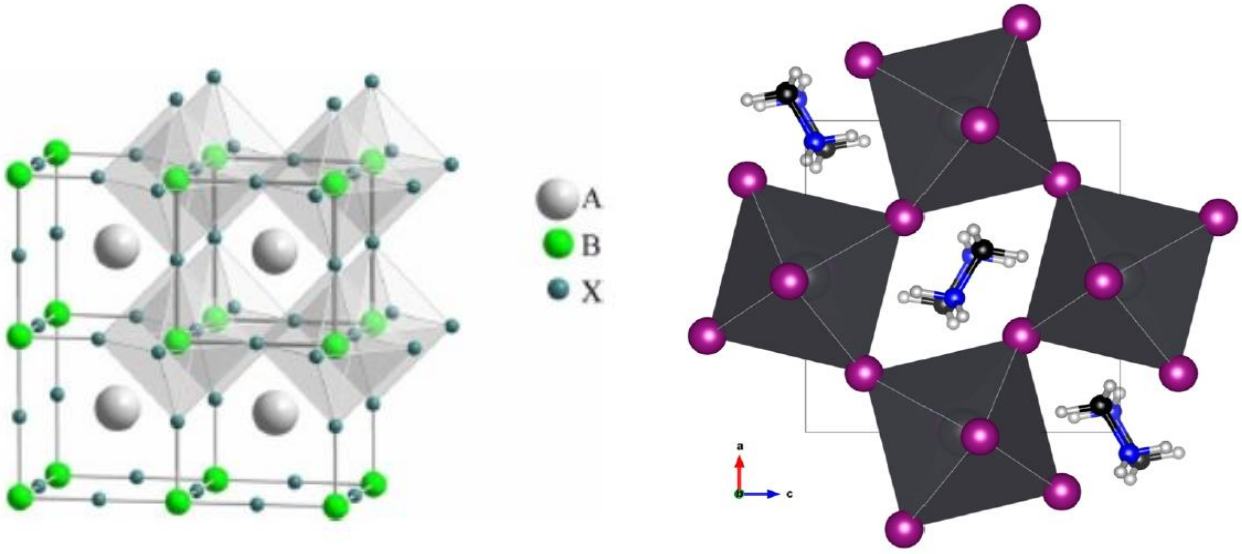

Figure 5.2(a): Generic ABX_3 perovskite crystal structure (left); Low temperature orthorhombic structure of $(MA)PbI_3$ with unit cell doubling, adapted from [30]

5.3 Photovoltaic performance

Despite the lack of information on the underlying basic photophysics responsible for the reported exceptional quality of hybrid Perovskites, as mentioned earlier – beginning with the early work by Miyasaka et al in in 2009 utilizing Perovskite absorbers in a dye-sensitized geometry, which yielded an efficiency of 3.8%, since then several groups have quickly pushed the limits to a certified 17.9%(NREL) using various strategies such as improved device architectures[38], new & highly efficient charge-carrier transporting materials and electrodes[39].These reports show that perovskites exhibit ambipolar transport characteristics and can therefore be used not only as light harvesting materials but also for charge transport.

Investigations by Snaith et al [35] and Sum et al [36], have partially ascribed this performance to extremely long exciton diffusion lengths in the solution processed Perovskites: $(MA)PbI_3$ and $(MA)PbI_xCl_{3-x}$ with values ranging between 0.1–1 μm, a figure far above values around 10nm from state-of-the-art low temperature solution processed organic photovoltaics. Reported values for the band gap of these highly efficient perovskite absorbers is around 1.55eV (800nm); interestingly,

photovoltages around 1.1V have also been reported [37] implying a small loss, most likely due to charge-carrier extraction or injection at the interface of the electrodes, the impressive exciton diffusion length, high photovoltage and ambipolar transport characteristics of Perovskites make them ideal candidates for highly efficient, cost effective PVs.

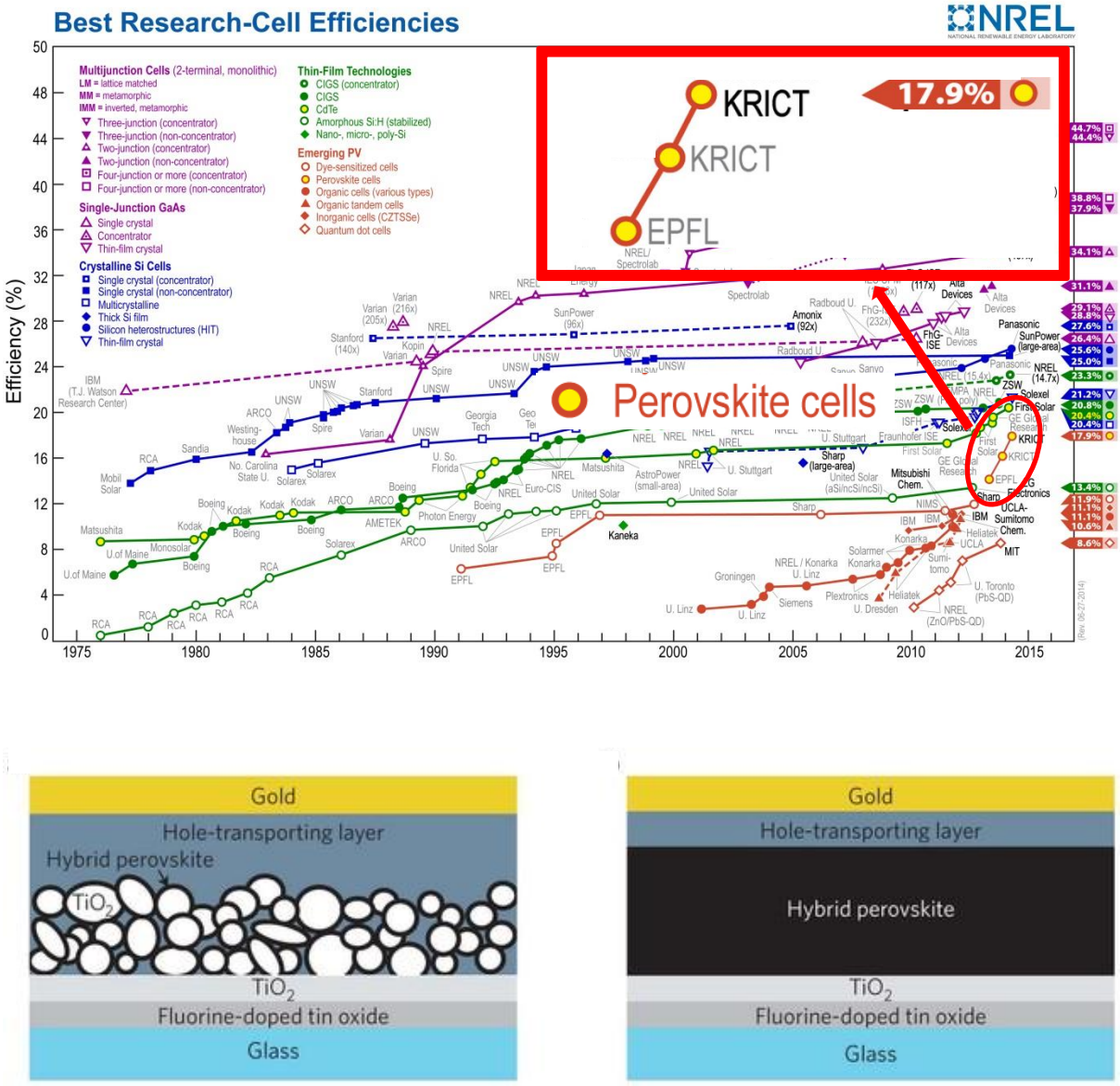

Fig 5.3(a): (top panel) The highest certified efficiency of perovskite solar cells of 17.9% by NREL as at the end of 2013 (credit: www.nrel.gov), reported by [32]. (bottom panel) Typical structures of perovskite based solar cells utilizing either a mesoporous TiO_2 layer or a planar geometry [20]

Chapter 6

Materials and Methods

$MAPbI_3$ single Crystals were synthesized from Methylammonium Iodide (MAI) and Lead (II) Iodide (PbI_2) using a simple drop-casting technique, described below.

6.1.1 Synthesis of Methylammonium Iodide (MAI)

MAI was synthesized by mixing 24 mL Methylamine (33% in ethanol) and 10 mL HI (57% in water) in 100 mL ethanol (in an ice bath) with constant stirring for 2 hours. After evaporation at 60°C in a hotplate, the resulting white powder was washed three times with ethyl ether and dried under vacuum at 60°C overnight.

6.1.2 Growing Single Crystals of Methylammonium Lead Iodide

Equimolar (1M) mixtures of PbI_2 and MAI of in gamma butyrolactone (10mL) were left to stir overnight at 60 °C. The single crystals were obtained by drop casting the solution on glass substrates. Then substrate was annealed at 100°C for 20 minutes.

*All materials used as purchased from sigma Aldrich

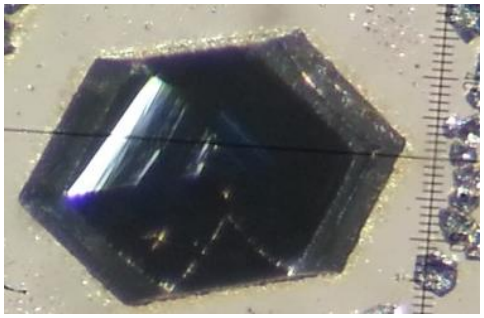

Fig 6.1.2(a): $MAPbI_3$ single crystal measuring (0.225 X 0.225 X 0.05)mm

6.2 Measurement Techniques

6.2.1 X-Ray Diffraction (XRD)

To further elucidate the structure of Perovskites, variable temperature XRD on both the single crystals and powered samples were carried out. XRD involves striking the sample with an intense beam of monochromatic X-rays, during which it is rotated and the reflections that arise are collected by a detector. Several thousands of reflections are collected and processed computationally to yield a model of the arrangement of atoms within the crystal, called the crystal structure. For single crystals of sufficient purity, XRD and complimentary chemical information can provide atomic coordinates, bond lengths and bond angles to a high degree of accuracy (tenths of Angstroms and tenths of degrees)

A few crystallographic studies of lead-halide based hybrid perovskites in literature [22] have pointed to cubic-tetragonal-orthorhombic phase transitions occurring as the Perovskite is cooled from above 330K to below 161K. These phase transitions are often attributed to the organic ligand (A) in the ABX_3 structure and is also likely to involve a distortion of the inorganic cage as well, the phase transition can be observed by performing XRD at multiple temperatures where different phases exist.

6.2.2 Photoluminescence (PL) and Time Resolved Photoluminescence Spectroscopy

Photoluminescence spectroscopy is one of the most important techniques for the optical characterization of semiconducting materials. It is a powerful, non-destructive method that gives information not only about the electronic structure of a material, but can also give insights about impurities in a semiconductor, provided their recombination is radiative [2]

Perovskites are extremely interesting materials for such measurements, because the nature of the fundamental photoexcitations and the origin of photoconductivity is yet unknown. PL experiments can help to elucidate the origins of fluorescence, which could be band-to-band recombination, from free excitons, bound excitons or even from impurity energy levels.

The dynamics of PL are also of great importance, and can be studied by time-resolved PL experiments, which involves measurement of the PL decay as a function of time after excitation by a pulsed monochromatic light source. Since band-to-band recombination dominates at room temperature and excitonic recombination is observed at lower temperatures [29], we measured the PL and TR-PL at temperatures ranging from 4K to 300K.

For our measurements, we used the second harmonic of a 150 fs mode-locked Ti:Sapphire laser at 795 nm with a repetition rate of ca. 76 MHz, pumped by a solid-state, diode-pump frequency doubled Nd:Vanadate (Nd:YVO4) laser at 532 nm with a output power of 5 Watts coupled to an optical pulse selector capable of working between 1:20 and 1:5000. All spectra were collected by a Hamamatsu EM-CCD camera sensitive in the visible range and time-resolved spectra were collected with a Hamamatsu streak camera with a photocathode sensitive in the visible range, working in single sweep mode. For low temperature measurements we used a continuous flow helium cryostat (He-flux-Oxford Optistat). All spectra were corrected for the optical response of the setup using a calibrated light source.

Chapter 7

Results and Discussion

7.1 X-Ray Diffraction

Powder X-ray Diffraction at room temperature (fig 7.1a) confirmed the successful synthesis of $MAPbI_3$, the experimental data and literature data agree very well. In addition, the absence of any unassigned peaks implies the absence of impurities.

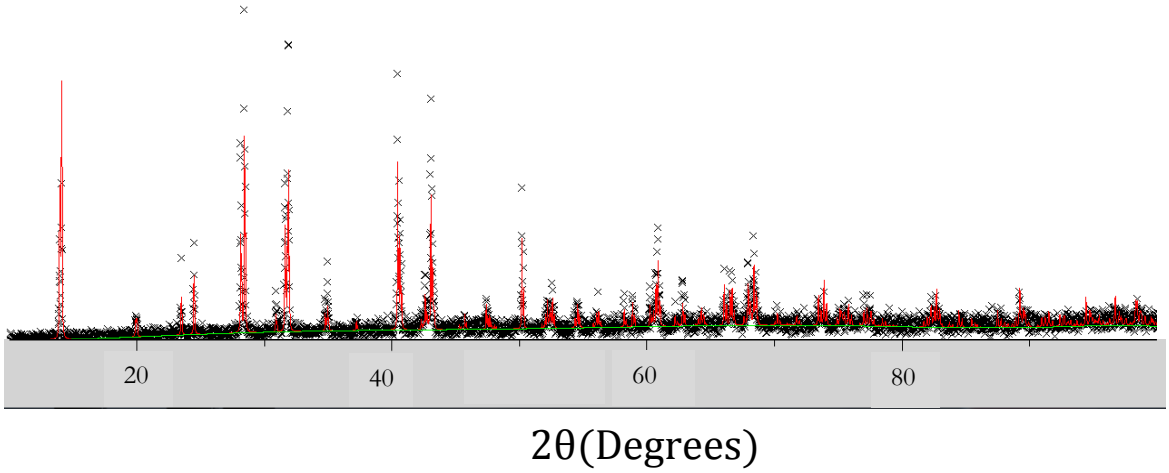

Figure 7.1(a): Powder XRD data at room tempreature, crosses represent experimental data and the red line indicates data from [31]

Furthermore, variable temperature single crystal XRD was carried out at temperatures between 200K and 130K; figure 7.3(b) below shows the diffraction pattern at 200K confirming the good quality of the grown crystals, the crystal structures at 200K and 130K (tetragonal and orthorhombic respectively) and extracted lattice parameters are shown in Figure (c)

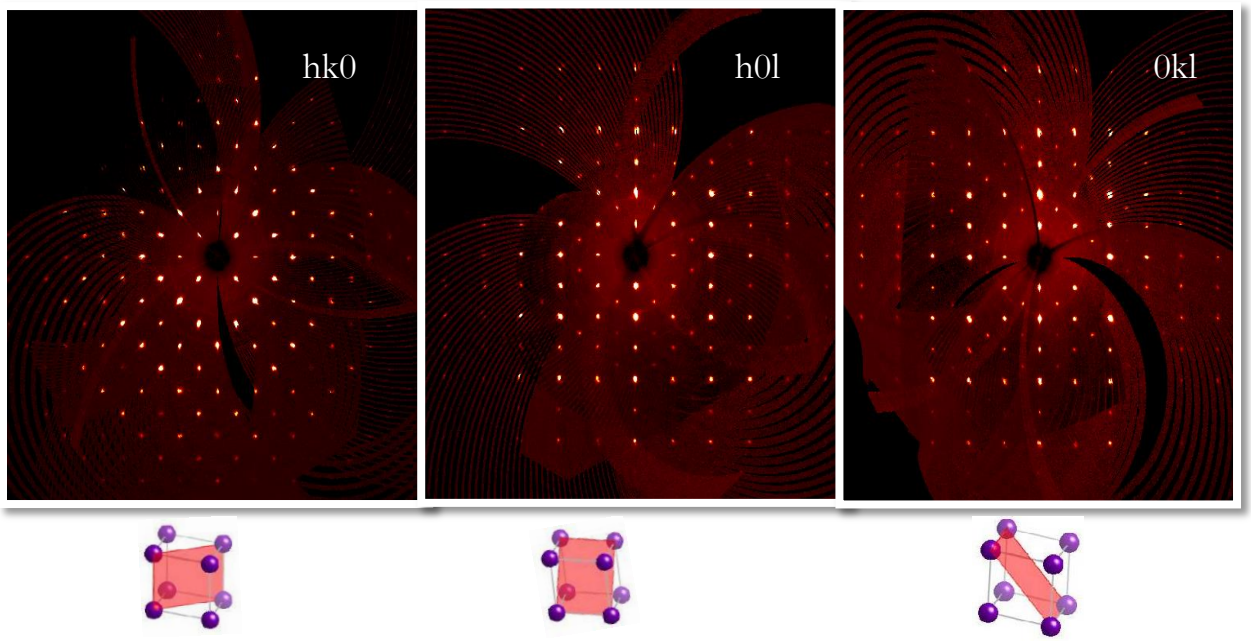

Fig 7.1(b) Single crystal XRD at 200K for different crystallographic planes, indicating the good quality of obtained crystals

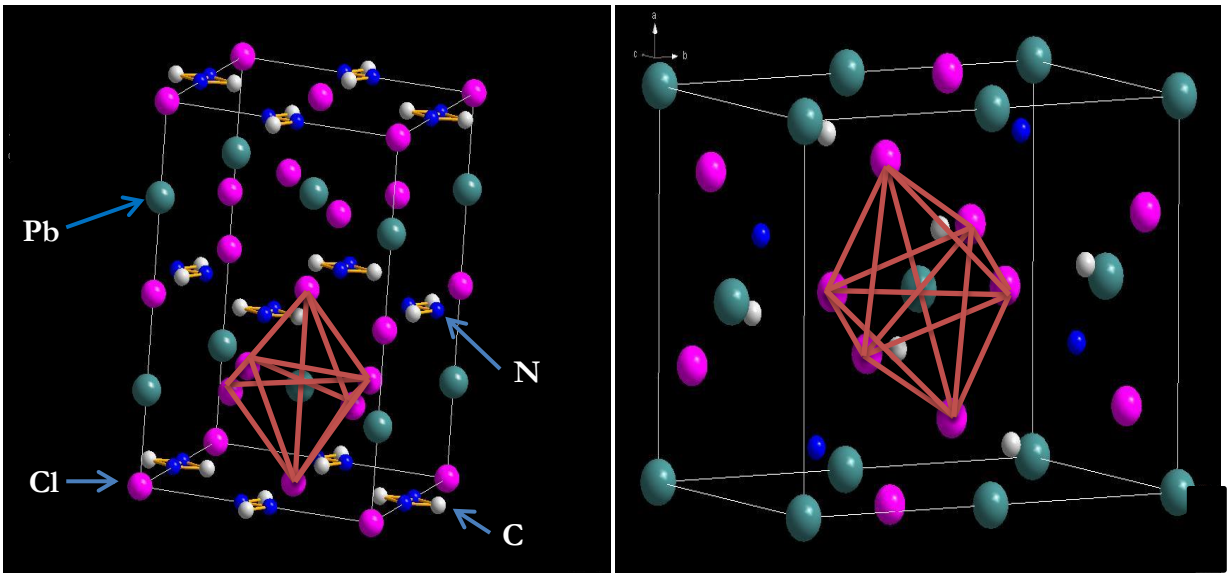

Structural Data		
Property	**Tetragonal**	**Orthorhombic**
Space Group	I422	Pnma
a (Å)	8.8155	8.7787
b (Å)	8.8155	8.6957
c (Å)	12.6165	12.561
$\alpha = \beta = \gamma$	90°	90°
V (Å^3)	980.43	958.87
Z	8	4

7.1(c): Crystal structures and parameters for the room temperature tetragonal phase and low temperature orthorhombic phase of $MAPbI_3$

Finally, in the vicinity of 162K, the emergence of new reflections (pictured below in fig 7.1d) confirms the tetragonal-orthorhombic phase transition.

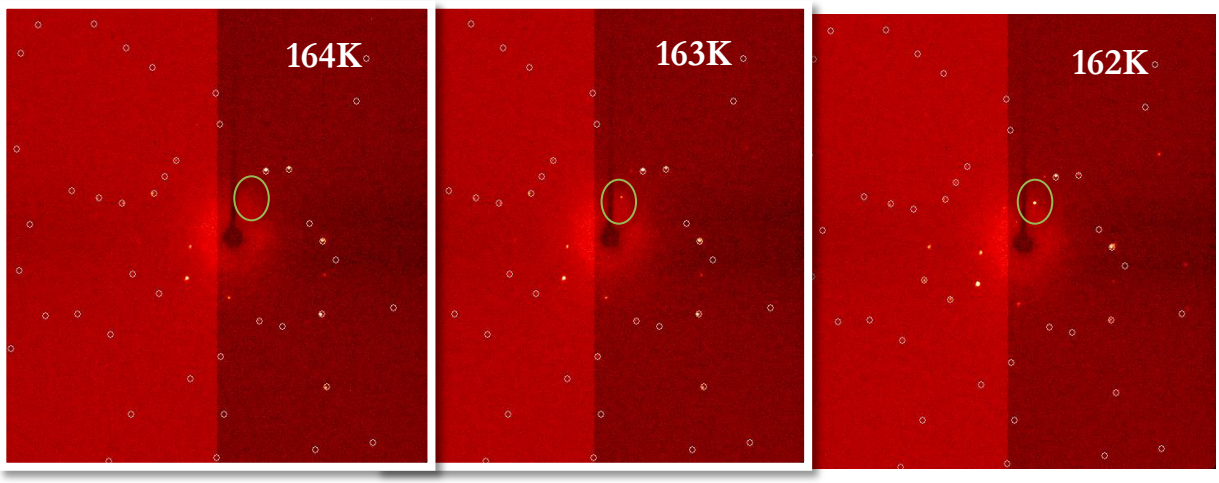

Fig 7.1(d): Diffraction patterns at temperatures around 162K, we observe the emergence of a new reflection (green circles) which is indicative of the tetragonal-orthorhombic phase transition

7.2 Steady State Photoluminescence Spectroscopy

As mentioned earlier, PL spectroscopy is a useful means of obtaining important information about several material properties such as the degree of crystallinity, quantum efficiency, presence of trap and defect states, recombination mechanisms and even phase transitions. All these information can be inferred from the intensity, line width and spectral content of photoluminescence collected.

$MAPBI_3$ has been known to exhibit two structural phase transitions [22,31], the first of which is cubic to tetragonal at elevated temperatures (approximately 330K) and the second, which is tetragonal to orthorhombic (at approximately 161K) which have both been attributed to the organic ligand (MA), though information about the exact nature of the phase transitions is still lacking in literature, we clearly observed the signature of the latter in our spectra at temperatures around 160K. Below this temperature, there are also several other interesting features in the PL contour map.

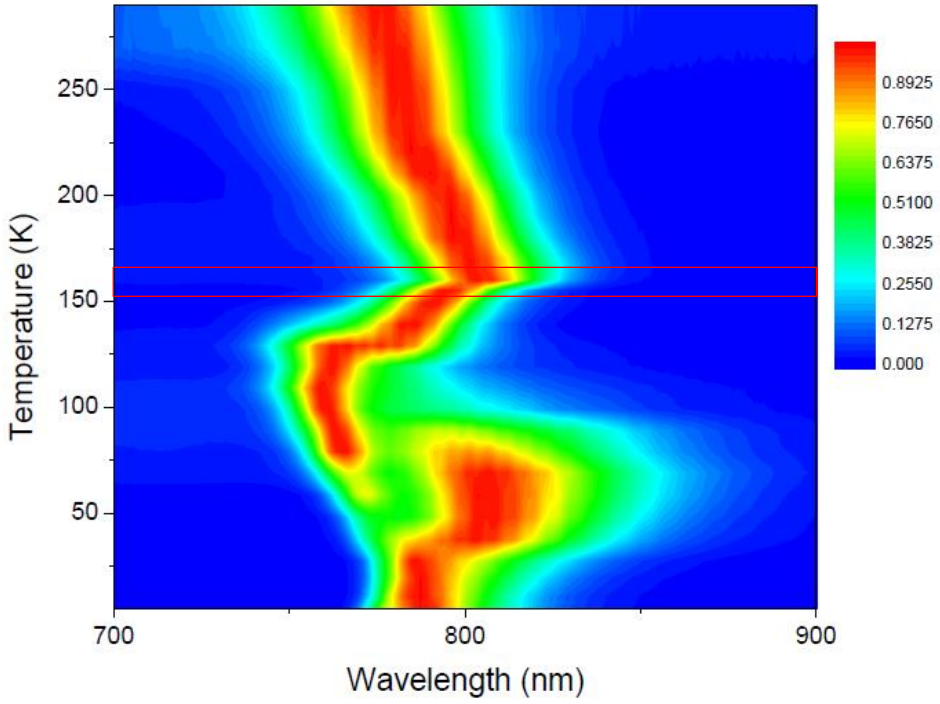

Fig 7.2(a): PL contour map for $MAPbI_3$ showing the variation in peak intensity and position with temperature, there is a phase transition around 162K (red box)

The figure (b) below shows an overview of selected spectra collected at different temperatures between 5K and 295K. What immediately strikes us is the variation in bandgap with temperature, usually described in inorganic semiconductors by the expression:

$$E_g(T) = E_g(0) - \frac{\alpha T^2}{T + \beta} \qquad (7.1)$$

Where E_g, α and β are fitting parameters. However, results by Kim and co-workers point to a variation in dielectric constant with temperature as a possibility for this observation [33]. This is affirmed by Poglitch & Weber, as well as Onada and co-workers [41, 42]; who point to dynamic disorder of the methyl-ammonium group in the room temperature phase, with successive ordering phenomena as cooling occurs. Thus, the dielectric constant varies with temperature which can then be directly related to a correlated tumbling of the carbon-nitrogen bond axis of the methyl-ammonium cation. Furthermore, the changes in the spectral shape as well as peak relative intensities at temperatures between 140K and 30K are noteworthy. We observe a slight bifurcation of the main PL peak and emergence of a shoulder around (140K – 120K) which grows in intensity at the expense of the main peak before reversing the trend and coalescing once again into a single peak below 30K.

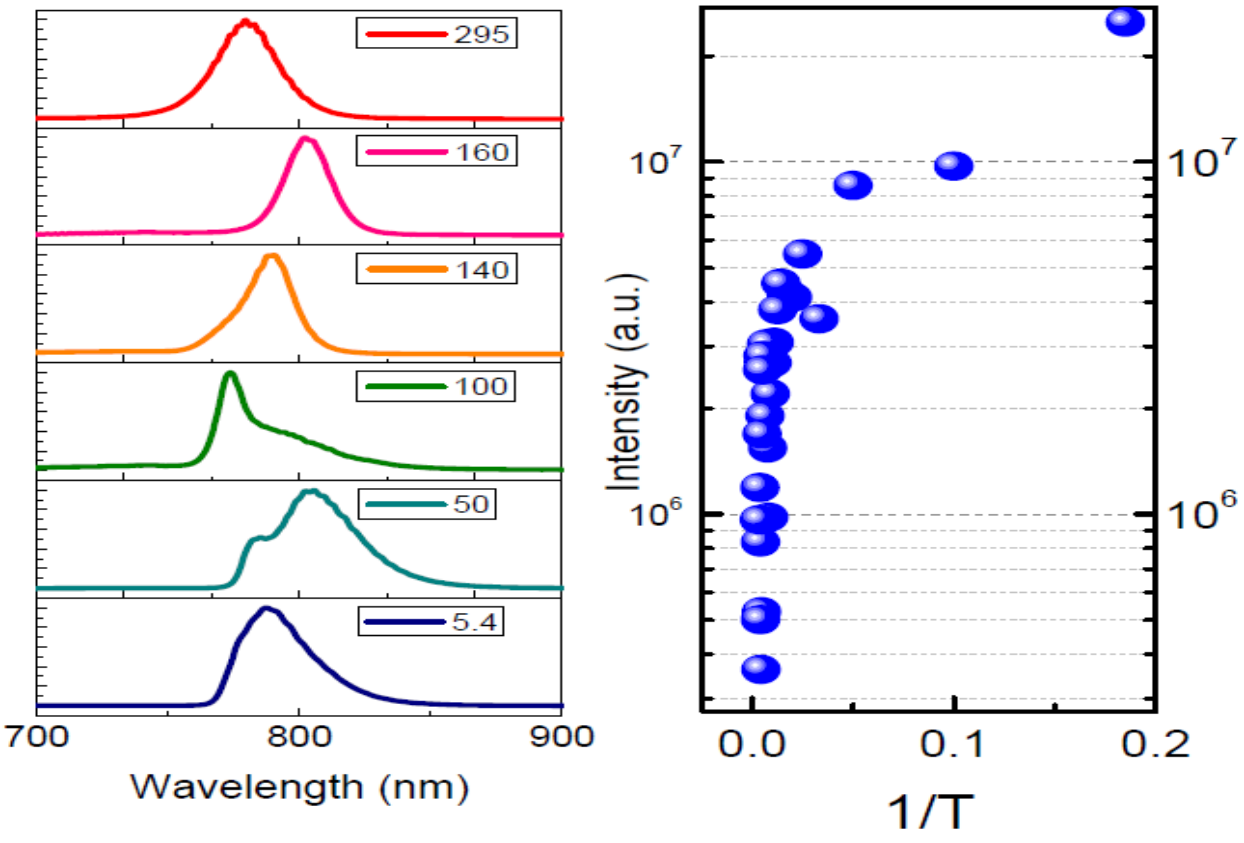

Fig 7.2(b): Normalized PL spectra at selected temperatures showing the changes that occur below the known phase transition at 162K, note the appearance of a shoulder at 140K which disappears below 30K (left), increase in intensity with decreasing temperature. Excitation intensity is approximately 40uW (right)

In figure (c) below, we report the results of power dependent measurements at several temperatures and observe that below 150K, the relative intensity of the main peak and shoulder change with increasing excitation intensity though with no clear trend observed across all temperatures; whereas at 100K and 50K, we observe a blue shift in the lower energy peak with increasing laser intensity.

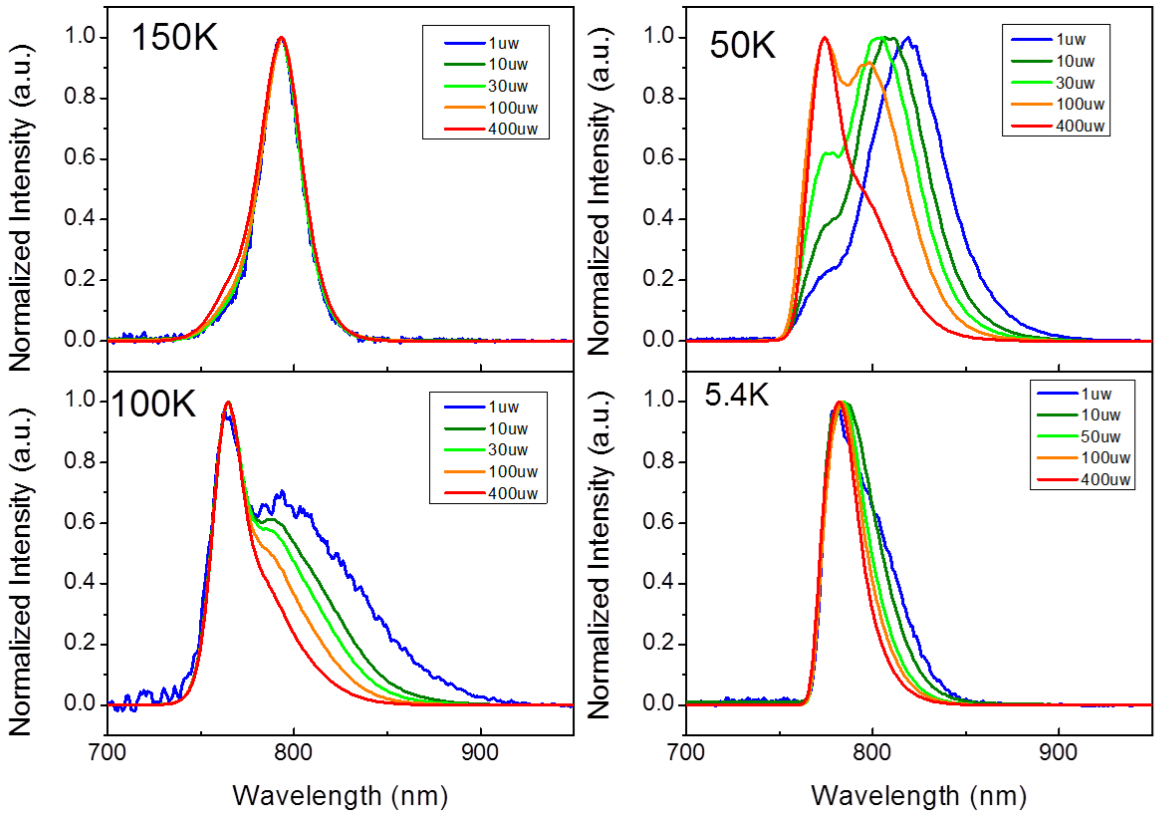

Fig 7.2(c): Power dependent measurements at selected temperatures below the phase transition; spectra are normalized

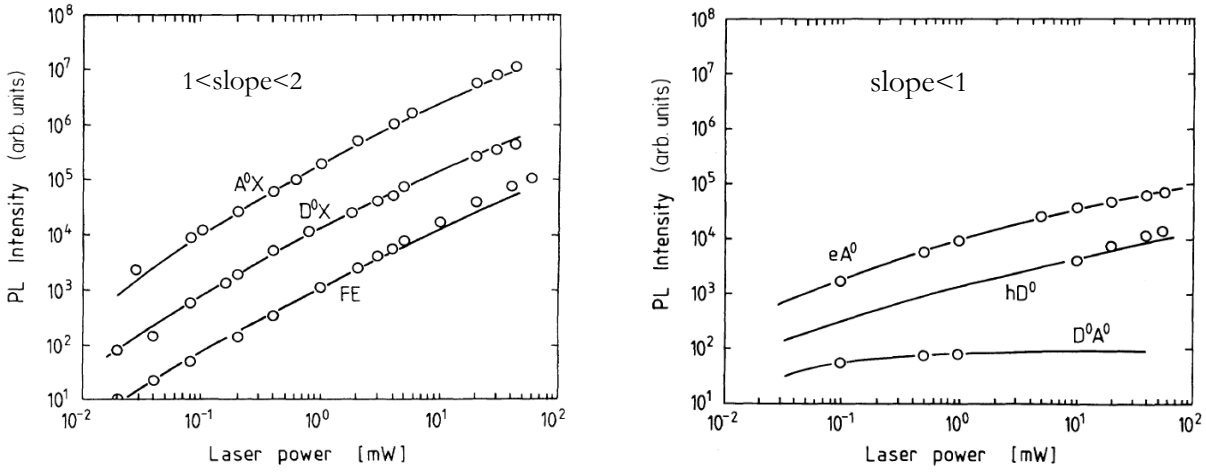

Fig 7.2(d): Results from [43] useful for discriminating between PL from traps and band-edge based on the excitation power dependence of the PL intensity. Left plot shows value of slope expected from free-, and bound-exciton emissions, right plot shows values expected from donor-acceptor, and free-to-bound (trap) recombination

The rationale behind power dependent measurements is to observe if any excitation-intensity dependent phenomena such as PL saturation occur. Previously, Katzer et al [28] reported saturation in the lower energy peak in the split PL spectra of quantum wells with increasing excitation intensity and ascribed it to state filling involving intra-bandgap impurity levels. In addition, theoretical work by Schimdt and Lischka [43] presents a general method for the discrimination between band-edge PL and that from impurities based the excitation power dependence. They proposed a general $I \sim L^k$ relationship between the luminescence intensity I and the excitation power L; with the slope k of the curve being between $k<1$ for luminescence from impurities (i.e. the so-called donor-acceptor pair recombination or a free-to-bound exciton recombination) as shown in figure 7.2(d). Since our measurements on $MAPbI_3$ do not reveal a straightforward state-filling signature (see figure 7.2(e) below); we therefore propose an explanation in terms of a multi-valley band structure with excited photo-carriers effectively moving between a saddle point and valleys in the valence band via an optical phonon assisted process as reported by calculations performed recently by Even et al [29].

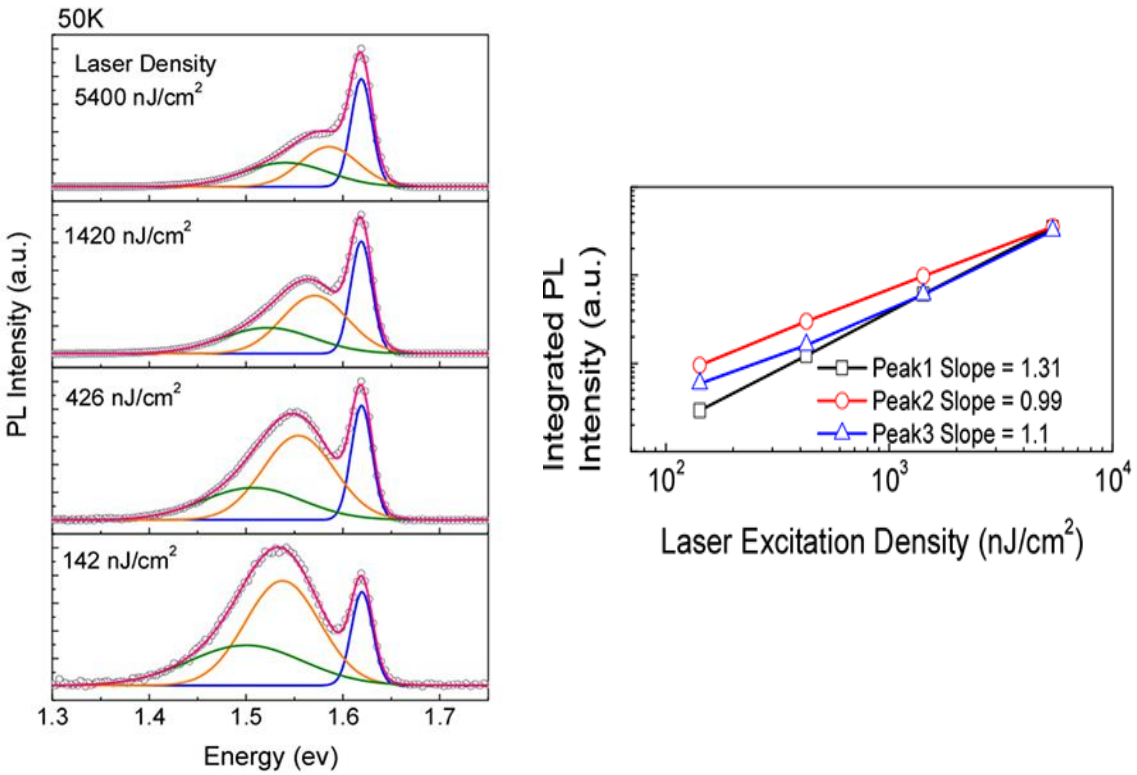

Fig 7.2(e): Excitation power dependence of PL from $MAPbI_3$ at 50K, this is representative of plots at other temperatures, the slopes for the curves suggest that we do not have PL from impurity energy levels, for which we would expect slope < 1

Their results suggest that the remarkable absorption, emission and transport properties of perovskites are possible by a multi-bandgap and multi-valley nature of their electronic band structure; they also propose that organic cations undergo collective motion which might be responsible for exciton screening, resulting in a predominance of free carriers over excitons at room temperature and hence improvement of transport properties.

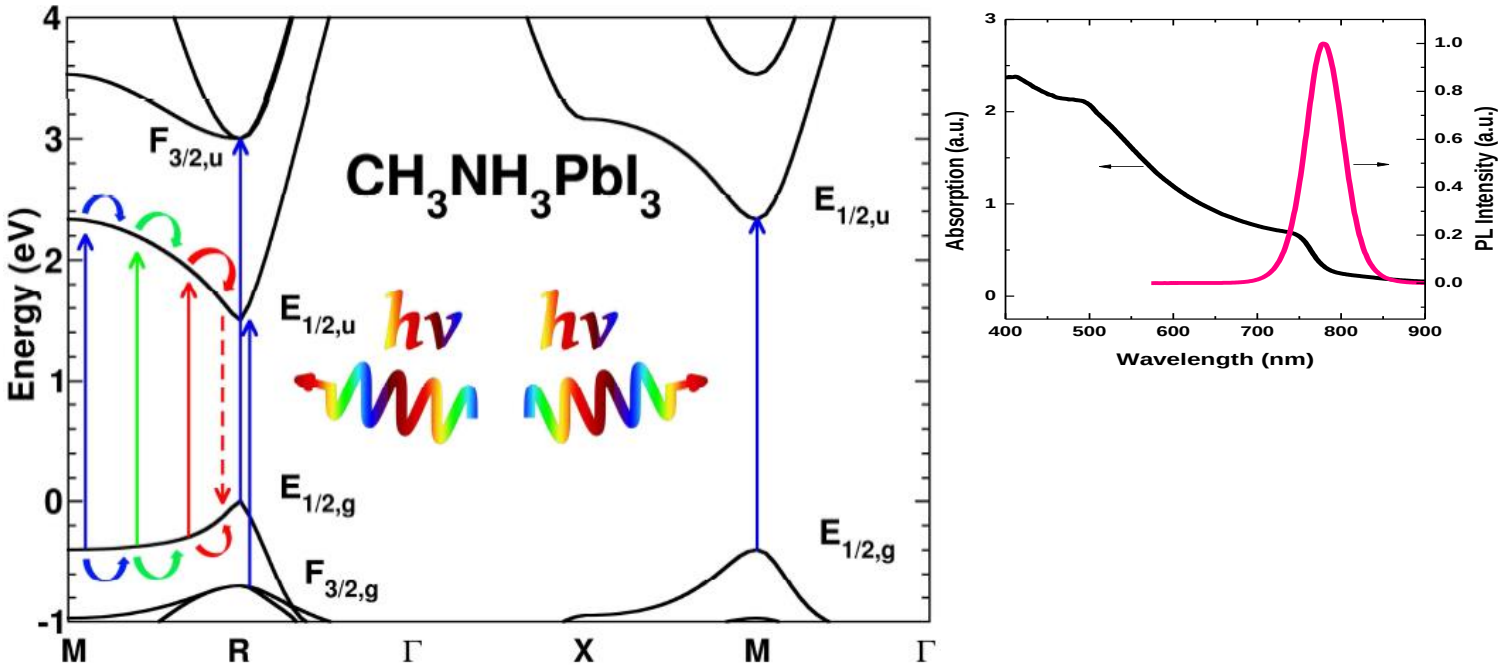

Fig 7.2(f): Band diagram for $MAPbI_3$ showing the multi gap and multi-valley character [29], inset shows absorption and PL spectra of films at room temperature, the absorption peak at 480 nm has been a source of debate for some time [25], the multi-bandgap scenario presented by in [29] explains its occurrence

Fig (f) suggests that both primary (R) and secondary (M) transitions are optically allowed, implying that optically generated carriers at M (with a larger optical matrix element) and all along the M→R path can flow towards E easily, assisted by acoustic phonons or via coupling to molecular rotations of the organic cation MA^+, this might explain the dual absorption peaks, and broad absorption spectra in perovskites which result in high photo-excitation efficiency in solar cells.

7.3 Time Resolved Photoluminescence Spectroscopy

While one of the most useful methods of understanding PL dynamics involves the analysis of quenching phenomena [28], it is also instructive to observe the trend of PL decay as a function of temperature as it can provide insights into the photo-conversion mechanism in $MAPI_3$ solar cells.

We measured the PL decay at various temperatures and observed a substantial increase in the lifetime (the time it takes the fluorescence to decay to $1/e$ of its initial value) from ca. 83ns at room temperature to 5367ns at 50K, with a slight decrease to 5043ns at 5K, we interpret this as an indication of high photoexcitation efficiency particularly when the crystal is cooled down. This is in very good agreement with results by Xing et al [25] and Stranks et al [24] who have measured diffusion lengths in the range of 0.1 – 1 μm using the drift diffusion model, with the diffusion length L given by $L = \sqrt{D\tau}$, where D is the diffusion coefficient and τ, the PL decay time.

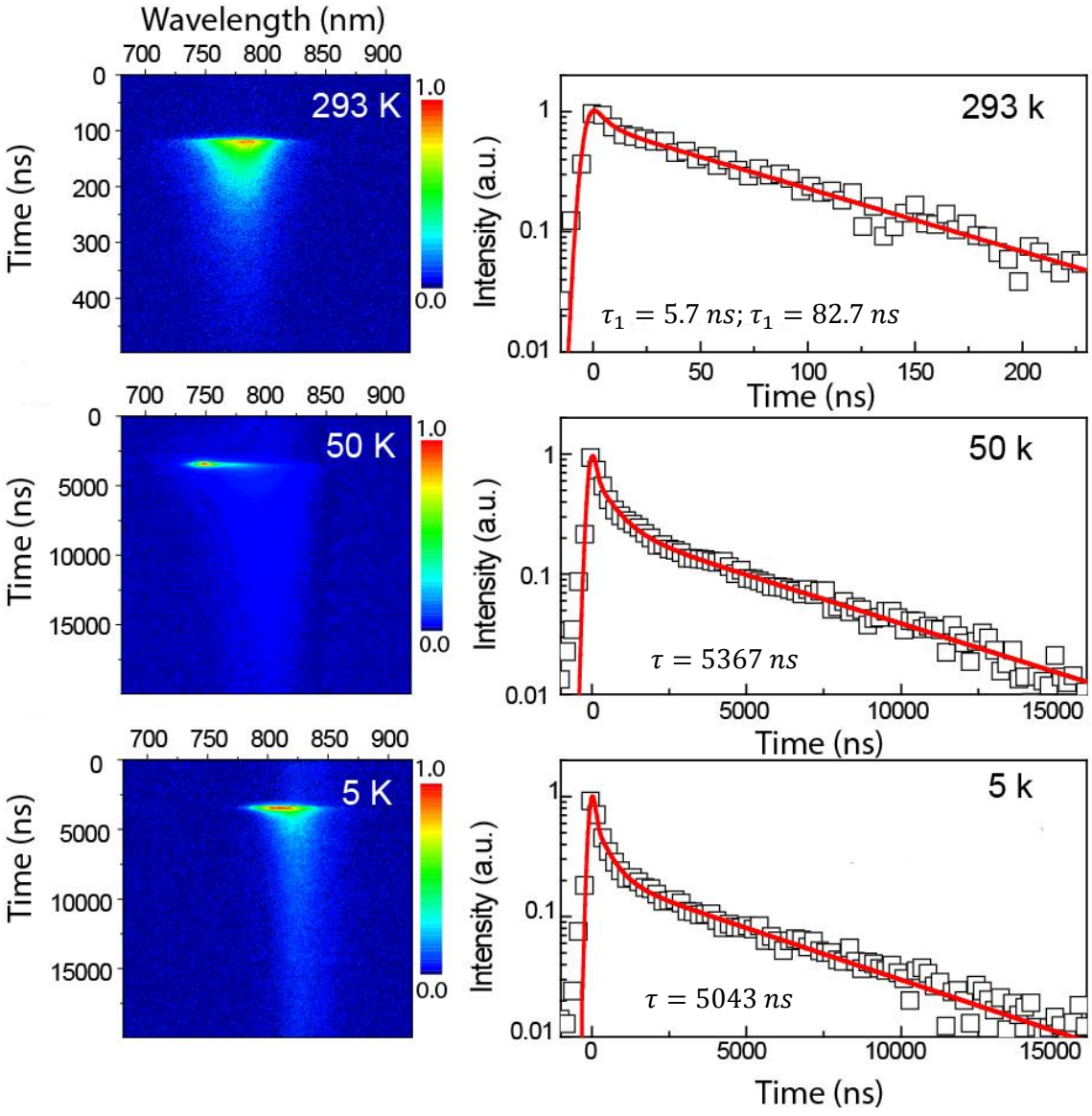

Figure 7.3(a) Time resolved PL spectra for $MAPbI_3$ showing streak camera traces in false color (left panel) and experimental data (black squares) with best exponential fits (red line) in the right panels

Chapter 8

Conclusion and Outlook

Organic-Inorganic hybrid perovskites are well-known materials that have been considered as excellent candidates for technological applications including: piezoelectricity, antiferromagnetism, and superconductivity and semi conductivity. Recently, several studies have shown them to be highly efficient in solar cell devices linked to their broad absorption in the visible and near-IR, long range balanced charge transport and high photo-excitation efficiency [29, 33, 35, 36]. Therefore, several studies point, rather optimistically to the possibility of using them as the "next big thing" in photovoltaic technology.

Despite their exceptional device performance reported recently, detailed information about their structure, physical and electronic properties vis-a-vis their device performance is still lacking. This study is part of a larger effort by our group and collaborators to improve our fundamental understanding of perovskites and also to pave the way for several improvements in device fabrication, charge extraction and material design.

Our findings underline that the solution processing route is a facile, viable option for the low cost synthesis of Perovskites (films and single crystals) particularly when high quality starting materials are used, confirmed by the absence of impurity peaks in our XRD spectra. We observe the tetrahedral-orthorhombic phase transition around 161K in our XRD spectra as new reflections in the single crystal diffraction pattern, which manifest in the steady state PL as a reversal in the observed trend of increasing emission wavelength with decreasing temperature. Furthermore, we report unusual changes in the PL spectra at temperatures around 150K, which then disappear below 30K.

Time resolved measurements show a large increase in PL lifetime by a factor of 60 between room temperature and 50K, with a slight decrease as the temperature further decreases to 5K. To the best of our knowledge, this has not been reported in literature before, and we take this as further proof of very high photoexcitation efficiency as reported in other studies.

In the future, we hope to continue efforts to optimize the fabrication of perovskite thin films for solar cells and also field-effect transistors (FETs) for studying charge carrier transport.

Acknowledgements

I have had a very memorable time studying in Groningen these past two years, I would like to thank the Zernike Institute for Advanced Materials, the Eric Bleumink fund and the Greenfield foundation for the opportunity to participate in the Topmaster program in Nanoscience, also all the professors who quickly fed my passion for science, and my classmates who have been not just been colleagues but very good friends as well.

This thesis would not have been possible without Prof. dr. M.A Loi, who gave me the opportunity to do research in her group and found the time to guide and advise me on both these projects and my career in general. Also, Dr. Honghua Fang and Dr. Satria Bisri have been extremely generous with their experience and have taught me many techniques that aided me greatly. Also, my gratitude goes to our collaborators at ETH Zurich: Prof. Maksym Kovalenko, and Olga Nazarenko who provided us with the CIS nanoparticles that formed the basis of part of this thesis

I would like to thank Widianta Gomulya and Marianna Manca, who spent several hours in the lab showing me the basics of spectroscopy; Raissa and Sampson Adjokatse, who synthesized the Perovskite samples; Dr Graeme Blake of Solid State Materials for Electronics (SSME) for help with the XRD measurements and all the other members of the Photophysics and Optoelectronics (POE) group, for help with sample preparation, explaining things I did not understand and for the wonderful working atmosphere; Finally I would like to thank Arjen Kamp, for technical support.

Finally, my love and eternal gratitude goes to my family and friends, whose unwavering support and emotional investments have allowed me come this far.

Alhamdulillah!

References

1. Sze, S. M.; Ng, K. K. Physics of semiconductor devices; John Wiley and Sons, 2007

2. Schroder, D. K. Semiconductor Material and Device Characterization (3rd ed.), Wiley (2006)

3. Lakowicz, J. R. Principles of Fluorescence Spectroscopy (3rd ed.) Springer (2006)

4. Park, J. and Kim, S.W. $CuInS_2$/ZnS core-shell quantum dots by cation exchange and their blue shifted photoluminescence. *J. Mater. Chem.*, 21, 3745-3750 (2011)

5. Deng, D., Chen, Y., Gu, Y. *et al* High-Quality $CuInS_2$/ZnS Quantum Dots for In vitro and In vivo Bioimaging. *Chem. Mater.*, 24, 3029-3037 (2012)

6. Szendrei, K. Charge Extraction from Colloidal Inorganic Nanocrystals. PhD thesis, University of Groningen, 2011.

7. Brus, L. E. A simple model for the ionization potential, electron affinity, and aqueous redox potentials of small semiconductor crystallites. *J. Chem. Phys.* 79, 5566 (1983)

8. Arici, E., Sariciftci, N. S. & Meissner, D. Hybrid Solar Cells Based on Nanoparticles of $CuInS_2$ in organic matrices. *Adv. Fun. Mater.*, 13(2), 165-171(2003)

9. Zhong, H., Lo, S. S., Scholes, G. D. *et al.* Noninjection Gram-Scale Synthesis of Monodisperse Pyramidal $CuInS_2$ Nanocrystals and Their Size-Dependent Properties. *ACS Nano*, 4(9), 5253-5262 (2010)

10. Song, W. & Yang, H. Efficient White-Light-Emitting Diodes Fabricated from Highly Fluorescent Copper Indium Sulfide Core/Shell Quantum Dots. *Chem. Mater.*, 24, 1961-1967 (2012)

11. Uehara, M., Watanabe, K., Tajiri, Y., Nakamura, H. & Maeda, H. Synthesis of $CuInS_2$ fluorescent nanocrystals and enhancement of fluorescence by controlling crystal defect. *J. Chem. Phys., 129, 134709*-(2008)

12. Zhang, S., Wei, S.-H., Zunger, A. & Katayama-Yoshida, H. Defect physics of the $CuInSe_2$ chalcopyrite semiconductor. *Phys. Rev. B.*, 57(16), 9642-9656 (1998)

13. Nose, K., Omata, T. & Otsuka-Yao-Matuso, S. Colloidal Synthesis of Ternary Copper Indium Diselenide Quantum Dots and Their Optical Properties. *J. Phys. Chem C.*, 113(9), 3455-3460(2009)

14. Li, L., Pandey, A., Klimov V. I. *et al.* Efficient synthesis of highly luminescent copper indium sulfide-based core/shell nanocrystals with surprisingly long-lived emission. *J. Am. Chem. Soc.,* 133**,** 1176–1179 (2011)

15. Hamanaka, Y. Kuzuya, T., Sumiyama, K. *et al.* Defect-induced photoluminescence and third-order nonlinear optical response of chemically synthesized chalcopyrite $CuInS_2$ nanoparticles. *Chem. Phys. Lett.* 466, 176-180 (2008)

16. Kolny-Olesiak, J. & Weller, H. Synthesis and Application of Colloidal $CuInS_2$ Semiconductor Nanocrystals. *ACS Appl. Mater. Interfaces*, 5, 12221-12237(2013)

17. Li, L., Daou, J. T., Reiss, P. *et al.* Highly Luminescent $CuInS_2$/ZnS Core/Shell Nanocrystals: Cadmium-Free Quantum Dots for In Vivo Imaging. *Chem. Mater,* 21, 2422-2429 (2009)

18. Pons, T., Pic, E., Dubertret, B. *et al.* Cadmium-Free $CuInS_2$/ZnS Quantum Dots for Sentinel Lymph Node Imaging with Reduced Toxicity. *ACS Nano*, 4(5), 2531-2538 (2010)

19. Mitzi, D. B. Progress Inorganic Chemistry; Ed by Karlin, K. D., Wiley, **43**, 1-121 (1999).

20. Loi, M. A. and Hummelen, J. C. Hybrid Solar Cells: Perovskites Under the Sun. *Nature Materials*, 12, 1087-1089 (2013)

21. D'Innocenzo, V., Grancini, G., Petrozza, A. *et al.* Excitons Vs Free Charges in Organo-Lead Tri-Halide Perovskites. *Nat. Comm.*, 5, 3586 (2014)

22. Baikie, T., Fang, Y., White, T. J. *et al.* Synthesis and Crystal Chemistry of the Hybrid Perovskite $(CH_3NH_3)PbI_3$ for Solid-State Sensitised Solar Cell Applications. *J. Mater. Chem. A*, 1, 5628 (2013)

23. Kojima, A., Teshima, K., Shirai, Y., & Miyasaka, T. Organometal Halide Perovskites as Visible-Light Sensitizers for Photovoltaic Cells. *J. Am. Chem. Soc.,* 131, 6050 (2009).

24. Stranks, S. D., Eperon, G. E., Snaith, H. J. *et al.* Electron-Hole Diffusion Lengths Exceeding 1 Micrometer in an Organometal Trihalide Perovskite Absorber. *Science*, 342, 341−344 (2013)

25. Xing, G., Mathews, N., Sum, T. C. *et al.* Long-Range Balanced Electron- and Hole-Transport Lengths in Organic-Inorganic $CH_3NH_3PbI_3$. *Science*, 342, 344−347 (2013)

26. Wehrenfennig, C., Mingzhen, L., Herz, L. M. *et al.* Homogeneous Emission Line Broadening in the Organo Lead Halide Perovskite $CH_3NH_3PbI_{3-x}Cl_x$. *J. Phys. Chem. Lett.*, 5, 1300−1306 (2014)

27. Gonzalez-Pedro, V., Juarez-Perez, E. J., Bisquert, J. *et al.* General Working Principles of $CH_3NH_3PbX_3$ Perovskite Solar Cells. *Nano Lett.*, 14, 888−893 (2014)

28. Gfroerer, T. H. Photoluminescence in Analysis of Surfaces and Interfaces. *Encyclopedia of Analytical Chemistry* ed. By R.A. Meyers, Wiley (2000)

29. Even, J., Pedesseau, L. and Katan, C. Analysis of Multivalley and Multibandgap Absorption and Enhancement of Free Carriers Related to Exciton Screening in Hybrid Perovskites. *J. Phys. Chem C*, 118, 11566-11572 (2014).

30. Even, J., Pedesseau, L., Jancu, J.-M. & Katan, C. Importance of Spin–Orbit Coupling in Hybrid Organic/Inorganic Perovskites for Photovoltaic Applications. *J. Phys. Chem. Lett.,* 4, 2999-3005 (2013).

31. Stoumpos, C. C., Malliakas, C. D. & Kanatzidis, M. G. Semiconducting Tin and Lead Iodide Perovskites with Organic Cations: Phase Transitions, High Mobilities and Near-Infrared Photoluminescent Properties. *Inorg. Chem*., 52, 9019-9038 (2013)

32. Ryu, S., Noh, J. H., Seok, S. I. *et al.* Voltage output of efficient Perovskite solar cells with high open-circuit voltage and fill factor. *Energy & Environmental Science,* 7**,** 2614-2618 (2014)

33. Kim, H. S., Im, S. H., and Park, N. –G. Organo-Lead Halide Perovskites: New Horizons in Solar Cell Research. *J. Phys. Chem. C*., 118, 5615 - 5625 (2014)

34. Service, R.F. Perovskite Solar Cells Keep Surging. *Science Magazine*, 344, 458 (2014)

35. Stranks, S. D., Eperon, G. E., Snaith, J. H. *et al.* Electron-hole diffusion lengths exceeding 1 micrometer in an organometal trihalide perovskite absorber. *Science*, 342, 341-344 (2013)

36. Xing, G., Mathews, N., Sum, C. T. *et al.* Long-range balanced electron-and hole-transport lengths in organic-inorganic $CH_3NH_3PbI_3$. *Science*, 342, 344-347 (2013)

37. Lee, M. M, Teuscher, J., Snaith J. H. et al. Efficient Hybrid Solar Cells Based on Meso-Superstructured Organometal Halide Perovskites, *Science,* 338, 643 (2012).

38. Kim H. S., Lee, C. R., Park, N. G. et al. Lead Iodide Perovskite Sensitized All-Solid-State Submicron Thin Film Mesoscopic Solar Cell with Efficiency Exceeding 9%. *Science. Rep.* 2, 591 (2012).

39. Liu, D., Kelly, T. L. Perovskite Solar Cells with a Planar Heterojunction Structure Prepared Using Room-temperature Solution Processing Techniques, *Nature Photonics,* 8, 133(2013).

40. Chen, B., Zhong, H., Bingsuo, Z. *et al.* Highly Emissive and Color-Tunable $CuInS_2$-Based Colloidal Semiconductor Nanocrystals: Off-Stoichiometry Effects and Improved Electroluminescence Performance. *Adv. Fun. Mater.* 22, 2081-2088 (2012)

41. Poglitsch, A. & Weber, D. Dynamic disorder in methylammouniumtrihalogenoplumbates(II) observed by millimetre-wave spectroscopy. *J. Chem. Phys.*, 87, 6373-6378(1987)

42. Onoda-Yamamuro, N., Matsuo, T. & Suga, H. Dielectric study of $CH_3NH_3PbX_3$ (X = Cl, Br, I). *J. Phys. Chem. Solids*, 53, 935-939(1992)

43. Schmidt, T. & Lischka, K. Excitation-power dependence of the near-band-edge photoluminescence of semiconductors. *Phys. Rev. B.*, 45(16), 8989-8994(1992)